Extensive and anomalous grounding-line retreat at Vanderford Glacier, Vincennes Bay, Wilkes Land, East Antarctica.

Hannah J. Picton[1*], Chris R. Stokes[1], Stewart S. R. Jamieson[1], Dana Floricioiu[2], Lukas Krieger[2]

[1]Department of Geography, Durham University, Durham, DH1 3LE, UK
[2]Remote Sensing Technology Institute, German Aerospace Center, Wessling, Germany

**Current address and correspondence to*: School of GeoSciences, University of Edinburgh, EH8 9XP, UK (hannah.picton@ed.ac.uk)

Abstract. Wilkes Land, East Antarctica, has been losing mass at an accelerating rate over recent decades in response to enhanced oceanic forcing. Overlying the Aurora Subglacial Basin, it has been referred to as the 'weak underbelly' of the East Antarctic Ice Sheet and is drained by several major outlet glaciers. Despite their potential importance, few of these glaciers have been studied in detail. This includes the six outlet glaciers which drain into Vincennes Bay, a region recently discovered to have the warmest intrusions of modified Circumpolar Deep Water (mCDW) ever recorded in East Antarctica. Here, we use satellite imagery, differential synthetic aperture radar interferometry (DInSAR) and remotely-sensed datasets of ice-surface velocity, ice-surface elevation and grounding-line position, to investigate ice dynamics between 1963 and 2022. Our results support previous observations of extensive grounding-line retreat at Vanderford Glacier, measured at 18.6 km between 1996 and 2020. The persistent grounding-line retreat, averaging 0.8 km yr^{-1}, places Vanderford Glacier as the fastest retreating glacier in East Antarctica, and the third fastest in Antarctica, across decadal time-scales. Such rapid retreat is consistent with the hypothesis that warm mCDW is able to access deep cavities formed below the Vanderford Ice Shelf, driving high rates of basal melting close to the grounding-line. With a retrograde slope observed inland along the Vanderford Trench, such oceanic forcing may have significant implications for the future stability of Vanderford Glacier.

1. Introduction

Mass loss from the Antarctic Ice Sheet (AIS), estimated to hold a sea level equivalent (SLE) of 57.9 ± 0.9 m (Morlighem et al., 2020), has accelerated over recent decades (Schröder et al., 2019). Whilst a range of AIS mass balance estimates have been made (Velicogna et al., 2014; Harig & Simons, 2015; McMillan et al., 2015; Martín-Español et al., 2016; Shepherd et al., 2019; Rignot et al., 2019; Schröder et al., 2019; Smith et al., 2020), a recent collation of 24 independent estimates indicates that the AIS lost a total of 2,720 ± 1,390 Gt of ice between 1992 and 2017 (The IMBIE Team, 2018). This negative mass balance was dominated by loss from the West Antarctic Ice Sheet (WAIS), averaged at a rate of -94 ± 27 Gt yr^{-1} over the same time period (The IMBIE Team, 2018).

Deleted: grounding line
Formatted: Font color: Auto
Deleted: University of
Formatted: Font color: Auto
Deleted: England
Formatted: Font color: Auto
Deleted: Scotland
Formatted: Font color: Auto
Deleted: remotely sensed optical
Deleted: satellite
Deleted:
Deleted:
Deleted: grounding line
Deleted: . Decadal trends in frontal position are observed across the Vincennes Bay outlet glaciers, potentially correlated to variations in sea ice production. Ice surface velocities were generally stable between 2000 and 2021, with some fluctuations measured across the grounding linegrounding-line of Bond East Glacier. Changes in ice surface elevation were spatially variable, but a clear and consistent thinning trend was measured at Vanderford Glacier between 2003 and 2020. Enhanced rates of ice thinning were seen across each of the Vanderford, Adams, Anzac, and Underwood Glaciers between 2017 and 2020. Most importantly,
Deleted: o
Deleted: confirm
Deleted: grounding line
Formatted: Font color: Auto
Formatted: Font color: Auto
Formatted: Font color: Auto
Formatted: Font color: Auto
Formatted: Font color: Auto
Deleted: Such rapid grounding linegrounding-line retreat (0.8 km yr^{-1})
Formatted: Font color: Auto
Deleted: notion
Formatted: Font color: Auto
Formatted: Font color: Auto
Deleted: .
Formatted: Font color: Auto
Deleted: ¶
Formatted: Font color: Auto

Recent mass loss from the WAIS (2000s to 2010s) has largely been concentrated within the Amundsen Sea Embayment (Harig & Simons, 2015; McMillan et al., 2015; Gardner et al., 2018; Shepherd et al., 2019), dominated by increased discharge from the fast-flowing Pine Island and Thwaites Glaciers (Mouginot et al., 2014; Medley et al., 2014; Christianson et al., 2016; Yu et al., 2018). The ice flow acceleration (Mouginot et al., 2014; Sutterley et al., 2014), dynamic thinning (Pritchard et al., 2009; Flament & Rémy, 2012) and rapid grounding-line retreat (Rignot et al., 2014) of these major outlet glaciers has been attributed to ice-shelf thinning (Pattyn & Morlighem, 2020). Such thinning reduces the buttressing force exerted by an ice-shelf and has primarily been attributed to basal melting, a process forced by the wind-driven intrusion of warm modified Circumpolar Deep Water (mCDW) across the continental shelf to sub-ice-shelf cavities (Feldmann & Levermann, 2015; Scambos et al., 2017; Rignot et al., 2019;). Situated on retrograde bed slopes grounded well below sea level, there has been widespread concern that the Pine Island and Thwaites Glaciers could be susceptible to marine ice sheet instability (MISI) (Joughin & Alley, 2011; Parizek et al., 2013; Nias et al., 2016; Lhermitte et al., 2020), whereby irreversible grounding-line retreat is triggered (Schoof, 2007). Indeed, Favier et al. (2014), Rignot et al. (2014) and Joughin et al. (2014) argue that such unstable retreat may already be underway.

In contrast, the recent mass balance of the East Antarctic Ice Sheet (EAIS), containing a SLE of 52.2 ± 0.7 m (Morlighem et al., 2020), has typically been estimated to either be in equilibrium (Schröder et al., 2019), or slightly positive (Martín- Español et al., 2016; Gardner et al., 2018; Shepherd et al., 2019; Smith et al., 2020; Stokes et al., 2022). The IMBIE Team (2018) calculated a positive mass balance of +5 ± 46 Gt yr^{-1} between 1992 and 2017, with mass gain predominantly concentrated in the Dronning Maud Land region (Velicogna et al., 2014; Harig & Simons, 2015; Martín-Español et al., 2016; Gardner et al., 2018). However, Rignot et al (2019) have instead suggested that the EAIS has been a significant contributor to recent sea level rise, with an estimated negative mass balance of -57.0 ± 2 Gt yr^{-1} between 1992 and 2017. Whilst the overall mass balance of the EAIS remains uncertain, numerous studies provide strong evidence of dynamic mass loss across the marine-based Wilkes Land sector (McMillan et al., 2015; Martín-Español et al., 2016; Smith et al., 2020; Stokes et al., 2022). Wang et al. (2021) have suggested that such mass loss has accelerated rapidly over the past two decades, increasing from -6 ± 22 Gt yr^{-1} between 2003 and 2008 to -51 ± 80 Gt yr^{-1} between 2016 and 2018. In addition, Miles et al. (2013) have observed widespread terminus retreat across the region, with 74% (n=39) of Wilkes Land outlet glaciers having undergone retreat at a median rate of -63.6 m yr^{-1} between 2000 and 2010.

Wilkes Land is characterised by a 'warm shelf' regime, whereby weak easterly winds and an absence of dense water formation facilitates the intrusion of warm CDW onto the continental shelf (Thompson et al., 2018; Stokes et al., 2022). The recent increase in mass loss across Wilkes Land has been linked to the enhanced intrusion of such CDW towards sub-ice shelf cavities, accessed through deep subglacial troughs (Miles et al., 2016; Shen et al., 2018). For example, increased ice discharge (Rignot et al., 2019) and dynamic thinning (Pritchard et al., 2009; Flament & Rémy, 2012; Li et al., 2016; Shepherd et al., 2019; Schröder et al., 2019) across the primary outlet of Wilkes Land, Totten Glacier (Figure 1b), has been attributed to enhanced

Deleted: e
Deleted: Feldmann & Levermann, 2015;
Deleted: driven
Deleted: grounding line
Deleted: and reduced buttressing,
Deleted:
Deleted: Pattyn & Morlighem, 2020
Deleted: that are
Deleted: grounding line
Deleted: m
Deleted: 2016
Deleted: measured to
Deleted: 2
Deleted: er

basal melt rates below the Totten Ice Shelf (Roberts et al., 2018; Pelle et al., 2021). Driven by increased intrusion of mCDW (Khazender et al., 2013; Gwyther et al., 2014; Spence et al., 2014; Li et al., 2015; Greene et al., 2017; Rignot et al., 2019), access to the main sub-ice-shelf cavity is provided by a deep inland subglacial trough (Greenbaum et al., 2015; Li et al., 2016). Such troughs are observed across the fjord landscape of the Aurora Subglacial Basin (ASB) over which Wilkes Land lies (Young et al., 2011; Miles et al., 2016).

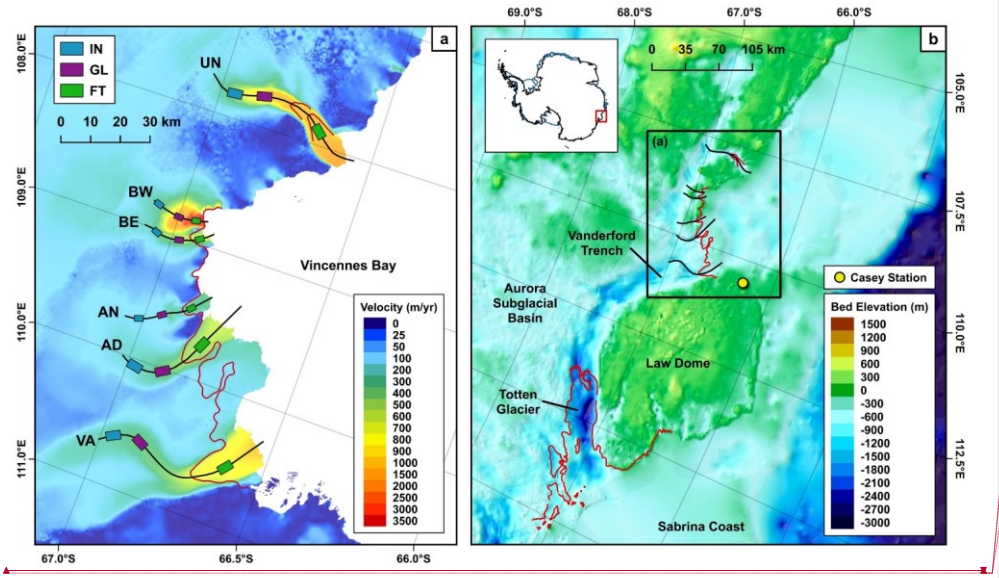

Figure 1. (a) Ice velocity map of Vincennes Bay extracted from the 2018 ITS_LIVE ice velocity mosaic (Gardner et al., 2022). Central flowlines are digitised along each of the studied glaciers: Vanderford (VA), Adams (AD), Anzac (AN), Bond East (BE), Bond West (BW), and Underwood (UN). Sampling boxes digitised across the inland (IN), grounding-line (GL) and floating tongue (FT) areas are shown. (b) Location map of Vincennes Bay and the Aurora Subglacial Basin. Background represents the bed elevation extracted from BedMachine (Morlighem, 2020), underlain by a hillshade. Inset map shows the location of the Aurora Subglacial Basin within Antarctica. Red lines in (a) and (b) display the 1996 MEaSUREs grounding-line product (Rignot et al., 2016).

The warmest intrusions of mCDW ever recorded within East Antarctica were observed within Vincennes Bay, defined as the shelf region situated on the Wilkes Land coast between 104° E and 111° E (Ribeiro et al., 2021). Vincennes Bay overlies the ASB and is drained by several marine-terminating outlet glaciers: Vanderford, Adams, Anzac, Bond, and Underwood (Figure 1a). Despite Rignot et al. (2019) briefly highlighting a dramatic 17 km retreat of Vanderford's grounding-line between 1996 and 2017, little attention has been afforded to these outlet glaciers. With area-averaged basal melt rates of 5.3 ± 2 m yr^{-1}

Deleted:
Formatted: Font color: Auto
Deleted:
Formatted: Font color: Auto
Deleted: down
Formatted: Font color: Auto
Deleted: grounding line
Deleted: and
Deleted: i
Deleted: grounding line
Deleted: noting
Formatted: Font color: Auto
Deleted: grounding line
Deleted: relatively high

estimated over the Vincennes Bay ice shelves (Rignot et al., 2013), Depoorter et al. (2013) had previously proposed that Vanderford may be vulnerable to oceanic forcing, potentially driven by the intrusion of mCDW. Indeed, recent analysis of data collected using instrumented seals revealed ocean temperatures higher than -0.5ºC are able to reach the Vanderford Ice Shelf, capable of driving basal melt (Ribeiro et al., 2021). Ribeiro et al. (2021) therefore suggested that a positive feedback may be initiated, whereby continued freshwater input from basal melt could hinder the formation of Dense Shelf Water (DSW) in the Vanderford polynya, thereby strengthening water column stratification and enabling the enhanced intrusion of warm mCDW at depth. Analysis by Herraiz-Borreguero & Garabato (2022) also suggests that this potential feedback may already be underway, with an observed decline in DSW concurrent with consistent sea ice production indicative of increased penetration of mCDW within the Vincennes Bay region. Whilst Vanderford Glacier is currently grounded on a prograde bedrock slope (Rignot et al., 2019), it overlies the Vanderford Trench, a deep subglacial trench characterised by an inland retrograde slope (Figure 1b) (Davis et al., 1986; Chen et al., 2011; Sun et al., 2016). Ice-sheet modelling indicates that grounding-line retreat beyond the present stabilising bedrock ridge could therefore facilitate MISI (Sun et al., 2016).

This paper seeks to improve our understanding of the largely unstudied Vincennes Bay outlet glaciers, providing an overview of recent ice dynamics observed between 1963 and 2022. We employ remotely sensed satellite imagery and a number of secondary datasets in order to analyse variation across four key glacier parameters: (1) terminus position, manually digitised from satellite imagery; (2) ice surface velocity, extracted from ITS_LIVE (Gardner et al., 2022) and ENVEO mosaics (ENVEO, 2021); (3) ice surface elevation, assessed using datasets produced by Schröder et al. (2019), Smith et al. (2020) and Nilsson et al. (2022); and (4) grounding-line position, newly mapped using DInSAR techniques and also extracted from datasets provided by Haran et al. (2005; 2014; 2018), Bindschadler et al. (2011) and Rignot et al. (2016).

2. Methods

2.1. Image Acquisition

A combination of Landsat 1, 4, 5, 7 and 8, Sentinel-2A and Sentinel-2B images (1973 – 2022) were downloaded from the USGS EarthExplorer data repository, with the majority of images selected from the austral summer months of December - February (Table S1). With each of the Vincennes Bay glaciers occupying a proportionally small area of each scene, cloud cover thresholds were not applied; instead, images were manually inspected to ensure cloud cover did not obscure the terminus. Each of the Landsat 1, 4 and 5 scenes were co-registered to a Sentinel-2B scene collected in 2021, in order to ensure consistent geolocation through time. Ground control points (GCPs) digitised across coastal rock outcrops, nunataks, and visibly stable ice features (Glasser et al., 2011) were used in order to apply a first-order polynomial transformation with nearest neighbour resampling (Miles, 2013). A mosaic of Antarctica composed of declassified ARGON satellite photographs collected in 1963 was also downloaded (Kim et al., 2007). This product has been orthorectified using GCPs (Kim et al., 2007), however the geolocation accuracy of the ARGON mosaic was manually checked before any subsequent analysis was conducted; the

Deleted:
Deleted: grounding line
Deleted: .
Formatted: Font color: Auto
Deleted:
Deleted:
Deleted: grounding line
Deleted: within
Deleted: .
Formatted: Font color: Auto
Deleted: then
Deleted: n
Deleted: orthorectified
Deleted:
Deleted:
Formatted: Font color: Auto
Formatted: Font color: Auto

position of coastal rock outcrops, nunataks, and visibly stable ice features was observed to be consistent with the Sentinel-2B scene collected in 2021. The spatial resolution of imagery used in this study therefore ranged between 10 and 140 m (Table S1).

2.2. Terminus Position

Annual terminus positions were manually digitised within QGIS. It should be noted that Bond Glacier has two distinct outlets separated by an ice rise; these two outlets are hereafter referred to as Bond East and Bond West (Figure 1). In May 2003, failure of the Scan Line Corrector onboard the Landsat 7 satellite resulted in striped data loss (Paul et al., 2017), but the majority of these gaps were observed to be perpendicular to the studied glacier termini. Thus, we were able to digitise terminus positions across the data gaps, with temporally close images with alternative striping patterns used in order to inform each digitisation (Black & Joughin, 2022). Once digitised, changes in terminus position were quantified by applying the well-established box method outlined by Moon & Joughin (2008). This method accounts for asymmetrical changes across glacier termini, using an open-ended box digitised across the main region of ice flow. Errors associated with this method of analysis arise from the co-registration of satellite imagery, generally estimated at 1 pixel, and manual digitisation of the terminus position, typically calculated as 0.5 pixels (Miles et al., 2018; Miles et al., 2021; Black & Joughin, 2022). Estimated errors associated with each terminus digitisation therefore ranged between 15 and 210 m (Table S1).

2.3. Ice Surface Velocity

With a lack of suitable data prior to 2000, the ITS_LIVE (Gardner et al., 2022) and ENVEO (ENVEO, 2021) datasets were used to extract ice-surface velocity between 2000 and 2021. ITS_LIVE velocity mosaics are available at an annual resolution between 2000 and 2018 and were derived from Landsat 4, 5, 7 and 8 imagery using the AutoRIFT feature tracking algorithm (Gardner et al., 2018). Each annual velocity mosaic has a spatial resolution of 240 m and reflects the error weighted average of all image-pairs with a centre date that falls within that calendar year (Gardner et al., 2022). In contrast, ENVEO velocity mosaics are provided at a monthly resolution between 2014 and 2021 and were derived from repeat-pass Sentinel-1 synthetic aperture radar (SAR) data using feature tracking techniques (Nagler et al., 2015; Nagler et al., 2021). Each of the monthly velocity mosaics has a spatial resolution of 200 m and was processed using the ENVEO software package (ENVEO, 2021). The monthly ENVEO velocity mosaics were used to extend our ice-surface velocity time-series, being downloaded between 2019 and 2021. In order to allow for comparison to the ITS_LIVE annual velocity mosaics, mean velocity across each 12-month period was calculated.

Ice surface velocity profiles were extracted along central flowlines manually digitised along each main glacier trunk (Figure 1a). Each longitudinal profile was sampled at an interval spacing of 240 m, reflecting the coarsest spatial resolution of the two velocity datasets used. To analyse changes in ice-surface velocity over time, mean annual velocity was extracted from within defined boxes for each given year. In order to assess the spatial variability in ice velocity, three sampling boxes were defined

Formatted: Font color: Auto

Deleted: hereafter

Deleted:

Deleted: ice surface

Deleted: auto-RIFT

Deleted: s

Deleted: 2019

Formatted: Font color: Auto

Deleted: In

Deleted:

Deleted: ice surface

across each glacier; the first box was positioned on the floating tongue (FT), the second located immediately up-glacier of the most landward observed grounding-line position (GL), and the third placed inland a further 5 km upstream (IN) (Figure 1a). Sampling boxes placed over the larger Vanderford, Adams and Underwood Glaciers each covered an area of 15 km^2, whilst sampling boxes placed across the smaller Anzac, Bond East, and Bond West Glaciers each had a proportionally smaller area of 6 km^2. Gardner et al. (2022) note that data scarcity is a significant limiting factor in the early ITS_LIVE product, with the auto-RIFT processing chain being limited by the number of image-pairs available across any given year. Such incomplete coverage was seen across the Vincennes Bay outlet glaciers, particularly prior to the launch of Landsat 8 in February 2013. Average annual velocity values were therefore only extracted from each respective FT, GL and IN box if greater than 25% data coverage was observed (Table S2).

The errors associated with each velocity measurement were also provided at the pixel scale. The mean velocity error was thus extracted from within each FT, GL and IN box across each given year. The velocity errors provided for each ITS_LIVE velocity mosaic were calculated according to the technical details outlined by Gardner et al. (2022). The errors are updated following co-registration and represent the standard deviation of the difference between the image-pair component velocities and the annual mean component velocities (Gardner et al., 2022). The uncertainty associated with each ENVEO velocity mosaic also represents the standard deviation (ENVEO, 2021). Velocity measurements were not included within the analysis if the mean error extracted across each box was calculated to be more than 50% of the mean velocity magnitude. However, this threshold resulted in the omission of just 5% of velocity measurements, largely concentrated across Bond West Glacier (Table S2).

2.4. Ice Surface Elevation

Variations in ice-surface elevation were analysed using the datasets provided by Schröder et al. (2019), Smith et al. (2020) and Nilsson et al. (2022). Schröder et al. (2019) calculated the monthly surface elevation change (SEC) observed between 1978 and 2017, relative to the reference month 09/2010. SEC measurements were provided at a horizontal resolution of 10 km and were obtained using combined altimetry data from each of the Seasat, Geosat, ERS-1, ERS-2, Envisat, ICESat and CryoSat-2 satellite missions (Schröder et al., 2019). Similarly, Nilsson et al. (2022) calculated the monthly SEC seen between 1985 and 2020, relative to the reference month 12/2013. Produced as part of NASA's ITS_LIVE project, SEC measurements were provided at a horizontal resolution of 1,920 m and included additional altimetry data from the ICESat-2 mission, launched in October 2018, thus facilitating further coverage between 2018 and 2020 (Nilsson et al., 2022). Mean monthly SEC values provided by both Schröder et al. (2019) and Nilsson et al. (2022) were extracted from each respective grounded GL and IN box. In order to allow comparison between the two datasets, all monthly SEC measurements were calculated relative to 09/1992, representing the earliest shared month for which data coverage was seen across all of the Vincennes Bay glaciers. Elevation anomalies were then calculated relative to the long-term means derived from each respective dataset between 1992 and 2017.

Deleted: grounding line

Deleted:

Deleted: ice surface

The ice-surface elevation dataset provided by Smith et al. (2020) represents the rate of SEC observed between 2003 and 2019, provided at a horizontal resolution of 5 km using altimetry data from the ICESat and ICESat-2 satellite missions. The mean rate of SEC observed over this period was extracted from each GL and IN box. In order to allow for comparison across all three elevation datasets, mean rates of SEC were also calculated from the monthly SEC data provided by Schröder et al. (2019) and Nilsson et al. (2022), extracted between 2003 and 2017 and 2003 and 2019, respectively.

2.5. Grounding-line Position

Grounding-line positions were delineated using differential satellite synthetic aperture radar interferometry (DInSAR) from ERS-1, ERS-2, and Sentinel-1 imagery collected between 1996 and 2020, processed as part of the European Space Agency's Antarctic Ice Sheet Climate Change Initiative (AIS CCI). The acquisitions used to complete grounding-line processing over the Vincennes Bay region are outlined in Table 1.

Satellite	Relative orbit/ Pass Direction	T1	T2	T3
ERS	231/D	1996-04-10	1996-04-11	-
Sentinel-1	133/D	2016-06-29	2016-07-11	2016-07-23
Sentinel-1	99/A	2017-07-22	2017-07-28	2017-08-03
Sentinel-1	99/A	2017-12-01	2017-12-07	2017-12-13
Sentinel-1	99/A	2017-12-07	2017-12-13	2017-12-19
Sentinel-1	70A	2020-11-13	2020-11-19	2020-11-25
Sentinel-1	70A	2020-11-19	2020-11-25	2020-12-01

Table 1. ERS and Sentinel-1 acquisitions used for interferogram generation in the Vincennes Bay region. Relative orbits and pass direction are stated, with A and D representing ascending and descending pass directions, respectively. T2 was chosen as the primary scene, with two interferograms T2-T1 and T2-T3 then formed. In the case of the ERS satellite, the grounding-line was delineated directly on a 1-day repeat pass interferogram.

The vertical motion of an ice-shelf and hence the hinge-line, representing the landward limit of ice flexure, can be observed from a single interferogram (Goldstein et al., 1993). The hinge-line is often used as a proxy for the grounding-line, the true position of which remains challenging to detect directly (Friedl et al., 2020). However, the exact location of the hinge-line is often obscured by the phase contributions of horizontal ice displacement. Therefore, we typically selected three repeat pass acquisitions in order to form two interferograms. The difference of such interferograms eliminates the phase contributions from horizontal ice displacement, when assuming a constant ice velocity throughout the observed time period (Rignot, 1996), revealing a dense fringe belt at the grounding zone. The landward limit of this fringe belt was manually delineated as the

Deleted: ice surface

Deleted: Grounding Line

Deleted:

Deleted: grounding line

Formatted: Font color: Auto

Formatted: Font color: Auto

Deleted:

Deleted:

Formatted: Font color: Auto

Deleted:

Deleted: d

interferometrically derived grounding-line position, with an estimated error of ± 200 m. Within the AIS CCI programme, a processing workflow has been developed to systematically map the grounding-line of the AIS using the Sentinel-1 SAR constellation. However, the repeat orbit of 6 and 12 days depends on the S1 observation plan. Wherever a 6-day repeat from a Sentinal-1 A and B combination was available, these acquisitions were favoured in order to limit temporal decorrelation due to changing surface conditions.

A number of secondary grounding-line datasets were also employed to enable comparison between datasets and to generate a higher temporal resolution of grounding-line positions (Table 2). The Making Earth Science Data Records for Use in Research Environments (MEaSUREs) grounding-line product was generated using similar DInSAR techniques as previously described for the AIS CCI product, also applied to ERS-1 and ERS-2 imagery collected in 1996 (Rignot et al., 2016). Whilst localised variations in positional accuracy are observed (Rignot et al., 2011), the MEaSUREs grounding-line product has an overall associated standard error of ± 100 m (Rignot et al., 2016) (Table 2).

Dataset	Date	Method	Error (m)
AIS CCI	1996 2016 2017 2020	Grounding-line derived using differential synthetic aperture radar interferometry from ERS-1, ERS-2, and Sentinel-1 imagery.	± 200
MEaSUREs (Rignot et al., 2016).	1996	Grounding-line derived using differential synthetic aperture radar interferometry from ERS-1 and ERS-2 imagery.	± 100
ASAID (Bindschadler et al., 2011)	2001 (1999 – 2003)	Manual digitisation of break-in-slope using observable change in image brightness from Landsat 7 imagery, aided by ICESat surface elevation profiles.	± 502
MOA (Haran et al., 2005; 2014; 2018)	2004 2009 2014	Manually digitised break-in-slope from contrast-enhanced imagery derived from the 2004, 2009 and 2014 Mosaics of Antarctica.	± 250

Table 2. Details of the different mapping methods employed to derive each of the grounding-line datasets used in this study. Note that the MEaSUREs, ASAID and MOA products represent secondary datasets.

The Antarctic Surface Accumulation and Ice Discharge (ASAID) grounding-line dataset was produced through manual delineation of the most seaward, spatially continuous break-in-slope, observed using a combination of Landsat-7 images collected between 1999 and 2003, and surface elevation data obtained from the ICESat satellite mission (Bindschadler et al., 2011). At outlet glacier boundaries such as those studied within Vincennes Bay, the ASAID grounding-line dataset had an estimated positional error of ± 502 m (Bindschadler et al., 2011). The Mosaic of Antarctica (MOA) grounding-lines were also provided through the manual digitisation of the most seaward break-in-slope, observed from the 2004 (Haran et al., 2005),

Deleted: grounding line
Deleted: grounding line

Satellite	Relative orbit/ Pass Direction
ERS	231/D
Sentinel-1	133/D
Sentinel-1	99/A
Sentinel-1	99/A
Sentinel-1	99/A
Sentinel-1	70A
Sentinel-1	70A

Deleted:
Table 1. ERS and Sentinel-1 acquisitions used for interferogram generation in the Vincennes Bay region. Relative orbits and pass direction are stated, with A and D representing ascending and descending pass directions, respectively. T2 was chosen as the primary scene, with two interferograms T2-T1 and T2-T3 then formed. In the case of the ERS satellite, the grounding ...
Formatted: Font color: Auto
Formatted: Font color: Auto
Deleted: grounding line
Deleted: grounding line
Deleted: grounding line
Deleted: provided
Deleted:
Formatted: Font color: Auto
Deleted: grounding line
Deleted: d
Deleted:
Formatted: Font color: Auto
Formatted: Font color: Auto
Deleted: grounding line
Deleted: grounding line
Deleted: provided
Deleted:
Deleted: grounding line
Deleted: grounding line

2009 (Haran et al., 2014), and 2014 (Haran et al., 2018) mosaics, respectively, each composed using MODIS imagery (Scambos et al., 2007). Each MOA grounding-line delineation therefore had an estimated associated error of ± 250 m (Haran et al., 2005; 2014; 2018), representing the ground-equivalent nadir pixel size of the MODIS bands (Scambos et al., 2007). Whilst the AIS CCI and MEaSUREs products both represent the hinge-line and thus approximate the actual grounding-line position (Fricker et al., 2009; Rignot et al., 2016), the ASAID and MOA datasets instead reflect the break-in-slope. This narrow region is observed seaward of the grounding-line and is typically inferred as the surface expression of the abrupt change in basal ice interface produced at the transition between grounded and floating ice (Scambos et al., 2007; Fricker et al., 2009; Bindschadler et al., 2011). The hinge-line and break-in-slope represent fundamentally different components of the grounding zone and therefore cannot be directly compared. Any observed grounding-line position change observed using the two different methods must thus be interpreted with caution, with further discussion restricted to pronounced signals and long-term trends that we can be confident are indicative of significant change.

In order to quantify changes in grounding-line position, changes were measured from the earliest 1996 delineation along each central flowline (Figure 1a). It should be highlighted that grounding-line positions at Vanderford Glacier in 1996 were provided by both AIS CCI and the MEaSUREs datasets, but were digitised in slightly different locations, approximately 640 m apart. Similarly, the MEaSUREs dataset also delineated two different 1996 grounding-line positions at Underwood Glacier, separated more significantly by ~ 7 km (Figure 1a). Whilst tidal effects may account for short-term migrations in grounding-line position (Rignot et al., 2016), both of the 1996 Underwood Glacier grounding-line positions provided in the MEaSUREs dataset were mapped using ERS imagery acquired on 6/2/1996, 7/2/1996, 12/3/1996, and 13/3/1996. The explanation for such significant geolocation variation therefore remains unknown. Conservative grounding-line retreat values were hence calculated for both Vanderford and Underwood Glacier, with retreat measured relative to the most landward observed 1996 position.

2.6. Bed and Ice Surface Topography

In order to assess the potential vulnerability to MISI, bedrock elevation profiles were derived from BedMachine (Morlighem, 2020) along each digitised flowline (Figure 1a). Bed elevation values and their associated errors were sampled at an interval spacing of 500 m, reflecting the horizontal resolution of the dataset. Whilst BedMachine was mostly mapped using mass conservation methods across regions of fast-moving ice, a range of different methods were employed across Vincennes Bay (Figure S1); the sampled errors therefore ranged between 10 and 202 m. Surface topography profiles were also extracted along each central flowline, sampled from the Reference Elevation Model of Antarctica (REMA) version 1 mosaic (Howat et al., 2019). The REMA v1 mosaic has a high spatial resolution of 2 – 8 m (Howat et al., 2019), however was sampled at the same 500 m interval spacing as the bed elevation.

Deleted: grounding line
Deleted: .
Deleted: inner limit of tidal flexure
Deleted: grounding line
Deleted: grounding line
Deleted: to be
Formatted: Font color: Auto
Deleted: ¶
Deleted: grounding line
Deleted: was
Formatted: Font color: Auto
Deleted: grounding line
Deleted: grounding line
Deleted: grounding line
Deleted: thus
Deleted: these glaciers
Deleted: obtained using
Deleted: were also extracted along each central flowline,

3. Results

3.1. Terminus Position

The terminus positions of the Vanderford, Adams, and Underwood Glaciers displayed the greatest variability across the Vincennes Bay outlet glaciers, fluctuating by ~7 km over the study period (Figure 2). Vanderford Glacier retreated ~4 km between 2007 and 2010, with a large extension of ice seen to protrude from the central terminus region (Figure 3a) being removed via calving. Following initial terminus advance, Adams Glacier showed a significant overall retreat, measured at ~6.3 km between 1973 and 2022 (Figure 2b). A spectacular disintegration of Underwood's floating tongue resulted in ~4.6 km of retreat between 2020 and 2022 (Figure 2f), with calved ice blocks clearly visible within the frontal sea-ice mélange (Figure 3f). The Bond East and Bond West termini were comparatively stable, fluctuating by a maximum of ~ 1.5 km over the study period (Figure 2). In clear contrast, Anzac Glacier exhibited an overall advance, measured at ~ 2 km between 1963 and 2022 (Figure 2c).

Deleted:

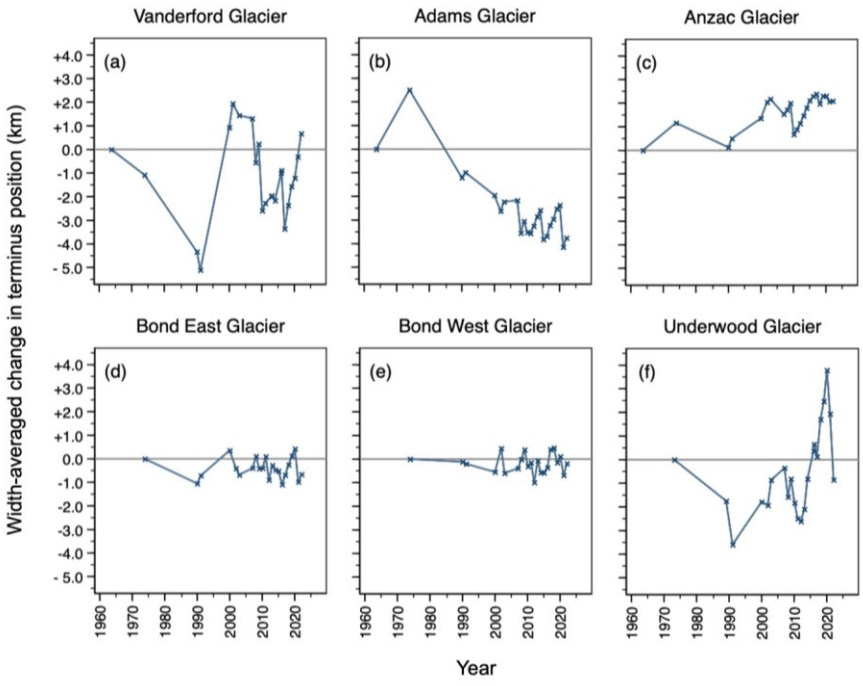

405

Figure 2. Width-averaged terminus position change observed relative to the first measurement point at a) Vanderford Glacier, b) Adams Glacier, c) Anzac Glacier, d) Bond East Glacier, e) Bond West Glacier, and f) Underwood Glacier. Note the raw time-series data of width-averaged terminus position change is provided in Table S3.

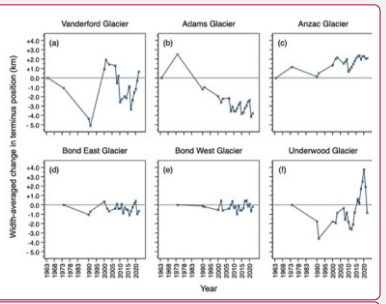

Deleted:

Formatted: Font color: Auto

Formatted: Font color: Auto

Deleted: displayed

Deleted:

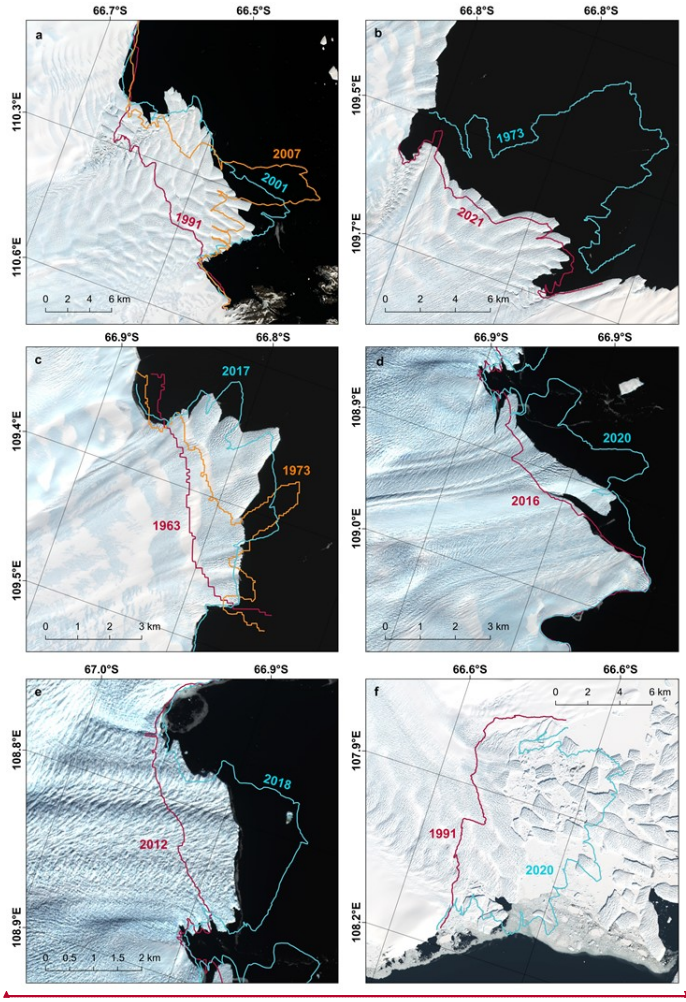

Figure 3. Minimum (red), maximum (blue), and notably asymmetrical (orange) terminus positions manually digitised across (a) Vanderford Glacier, (b) Adams Glacier, (c) Anzac Glacier, (d) Bond East Glacier, (e) Bond West Glacier, and (f) Underwood Glacier. All background satellite imagery displayed was collected from Sentinel-2B in February 2022, downloaded from the USGS EarthExplorer data repository.

Formatted: Font color: Auto

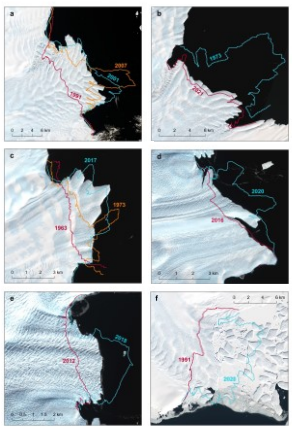

Deleted:

Formatted: Font color: Auto

Deleted: .

At the decadal scale, the Vincennes Bay outlet glaciers fluctuated between periods of largely synchronous terminus retreat and terminus advance. Between 1973 and 1991, each of the six glaciers showed an overall retreat, calculated at a median rate of -116.8 m yr^{-1} (Table 3). In contrast, between 1991 and 2000, four glaciers were observed to advance, with a positive median rate of terminus position change of +106.8 m yr^{-1} calculated across the six glaciers. Between 2000 and 2012, all six glaciers showed an overall retreat, calculated at a median rate of -86.3 m yr^{-1}. Between 2012 and 2022, five glaciers were recorded to advance, with a median rate of +88.1 m yr^{-1} observed across the Vincennes Bay outlet glaciers.

Rate of width-averaged terminus position change (m yr^{-1})

	1973 - 1991	1991 - 2000	2000 - 2012	2012 - 2022
Mean	-117.4	+156.5	-96.6	+98.6
Median	-116.8	+106.8	-86.3	+88.1
STD	97.8	275.3	80.5	111.7

Table 3. Rate of width-averaged terminus position change observed across the Vincennes Bay outlet glaciers. Note that the raw time-series data of width-averaged terminus position change is provided in Table S3.

3.2. Ice Surface Velocity

Significant variability in ice surface velocity was observed between the Vincennes Bay outlet glaciers (Figure 1a), with spatial variations also seen along-flow at each glacier (Figure 4). In 2018, Anzac Glacier was measured to be the slowest flowing outlet glacier, with velocity increasing from 128 ± 1 m yr^{-1} inland at AN (Figure 1a) to a maximum of 331 ± 1 m yr^{-1} at the terminus (Figure 4c). In contrast, Bond West was measured to be the fastest flowing outlet glacier, accelerating rapidly from 241 ± 4 m yr^{-1} inland at BW (Figure 1a) to a maximum velocity of 3,339 ± 2 m yr^{-1} (Figure 4e), representing one of the highest recorded velocities within Antarctica. The maximum velocity measured across each of the Vanderford, Adams, Bond East and Underwood Glaciers ranged from 598 ± 1 to 1,625 ± 4 m yr^{-1} (Figure 4).

Deleted: thus

Deleted:

Formatted: Font color: Auto

Formatted: Font color: Auto

Deleted: ice surface

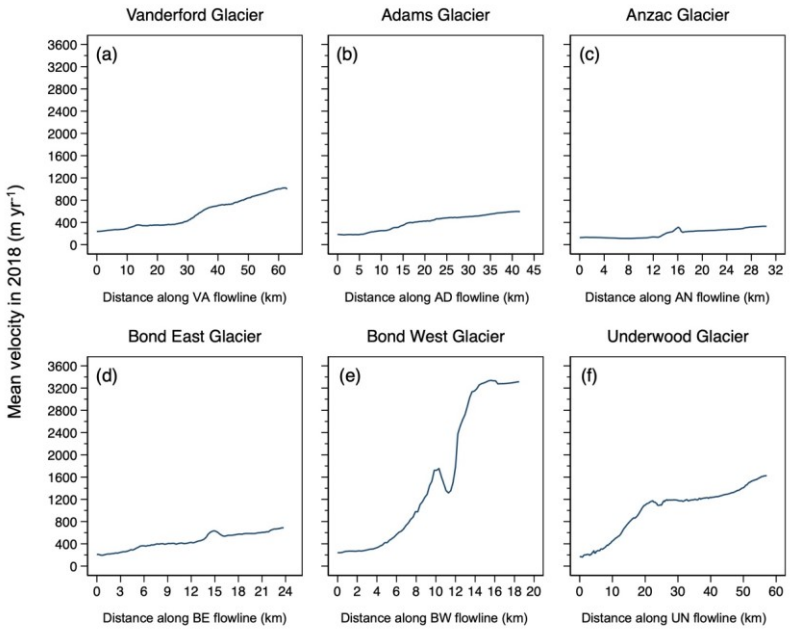

Figure 4. Ice surface velocity profiles extracted using the ITS_LIVE 2018 velocity mosaic (Gardner et al., 2022) along the central flowlines of (a) Vanderford Glacier, (b) Adams Glacier, (c) Anzac Glacier, (d) Bond East Glacier, (e) Bond West Glacier, and (f) Underwood Glacier. Note that distance is measured in the along-flow direction, with 0 km representing the inland start point of each respective flowline.

Temporal variations in ice-surface velocity were limited over the observational period (Figure 5) with ice-surface velocity showing no major changes across each of the Adams, Bond West, and Underwood Glaciers. Whilst ice-surface velocity was seen to increase by 12% across the FT of Anzac Glacier between 2009 and 2021 (Figure 5c), this velocity increase was not deemed notable, with the absolute value of acceleration (30 m yr^{-1}) being smaller than the associated error (± 82 m yr^{-1}). However, a clear 31% increase was observed at Vanderford Glacier, with ice-surface velocity at box IN accelerating from 201 ± 39 to 264 ± 6 m yr^{-1} between 2000 and 2013 (Figure 5a). Significant variations were also seen at Bond East Glacier, with a period of deceleration measured between 2006 and 2009, followed by a subsequent acceleration between 2009 and 2021 (Figure 5d). Such variation in ice-surface velocity was consistent across each of the IN, GL, and FT boxes. At the GL box, ice-surface velocity slowed by 15%, decreasing from 508 ± 42 m yr^{-1} in 2006 to 430 ± 66 m yr^{-1} in 2009 (Figure 5d). Subsequent acceleration was also calculated at 15%, with ice-surface velocity observed to increase to 496 m yr^{-1} in 2021 (Figure 5d).

Deleted:
Formatted: Font color: Auto
Formatted: Font color: Auto
Deleted: downstream
Formatted: Font color: Auto
Deleted: ice surface
Deleted: ice surface
Deleted: ice surface
Deleted: .
Deleted: ice surface
Deleted: recorded to accelerate
Deleted: ice surface
Deleted: ice surface
Deleted: ice surface

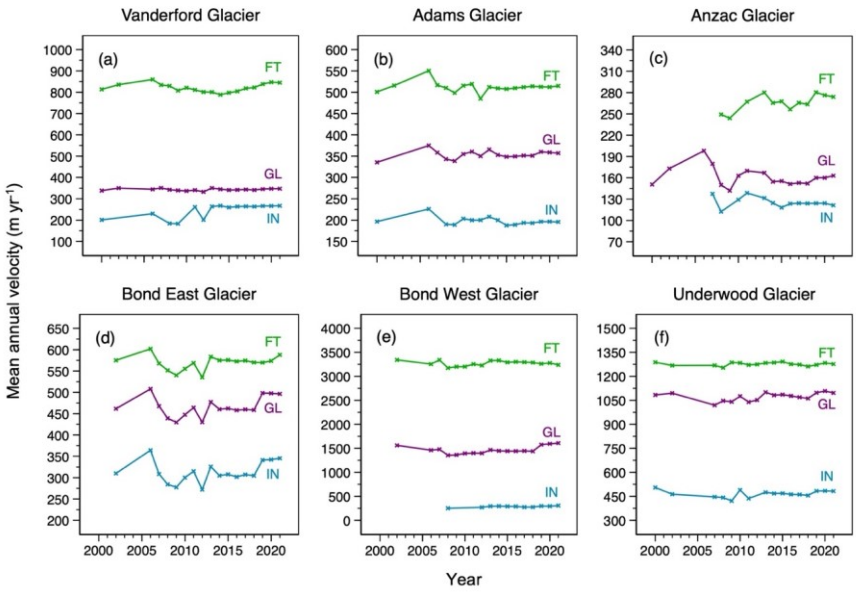

Figure 5. Mean annual velocity extracted within the inland (IN), grounding-line (GL) and floating tongue (FT) boxes across (a) Vanderford Glacier, (b) Adams Glacier, (c) Anzac Glacier, (d) Bond East Glacier, (e) Bond West Glacier, and (f) Underwood Glacier. Velocity data extracted from the ITS_LIVE velocity mosaics between 2000 and 2018 (Gardner et al., 2022) and ENVEO datasets between 2019 and 2021 (ENVEO, 2021). Note the different scales on the y-axes.

3.3. Ice Surface Elevation

The ice-surface elevation data provided by both Schröder et al. (2019) and Nilsson et al. (2022) were associated with high levels of uncertainty prior to 2003, particularly during the early 1990s (Figure 6). However, with the exception of Anzac Glacier (Figure 6c), there was a general agreement between each respective dataset regarding the overall pattern of ice-surface elevation change measured across each GL box. A clear and consistent thinning trend was measured at Vanderford Glacier throughout the observational period (Figure 6a). Between 2003 and 2017, Schröder et al. (2019) and Nilsson et al. (2022) observed thinning at an average rate of -0.12 and -0.07 m yr^{-1}, respectively. However, Nilsson et al. (2022) observed an enhanced rate of thinning between 2017 and 2020, measured at -0.22 m yr^{-1}. Despite their observed stability between 2003 and 2017, Nilsson et al. (2022) also measured enhanced rates thinning rates across the Adams, Anzac, and Underwood Glaciers

Formatted: Font color: Auto

Formatted: Font color: Auto

Deleted: grounding line

Deleted: ice surface

Deleted: ice surface

Deleted:

between 2017 and 2020 (Figure 6), calculated at an average rate of -0.32, -0.44, and -0.38 m yr^{-1}, respectively. In contrast, ice-surface elevation was observed to be stable across both Bond East and Bond West between 2003 and 2020, with Nilsson et al. (2022) measuring minor thickening at an average rate of just +0.01 m yr^{-1}. The patterns of surface elevation change were observed to be consistent across both the GL (Figure 6) and IN (Figure S2) boxes at each respective glacier.

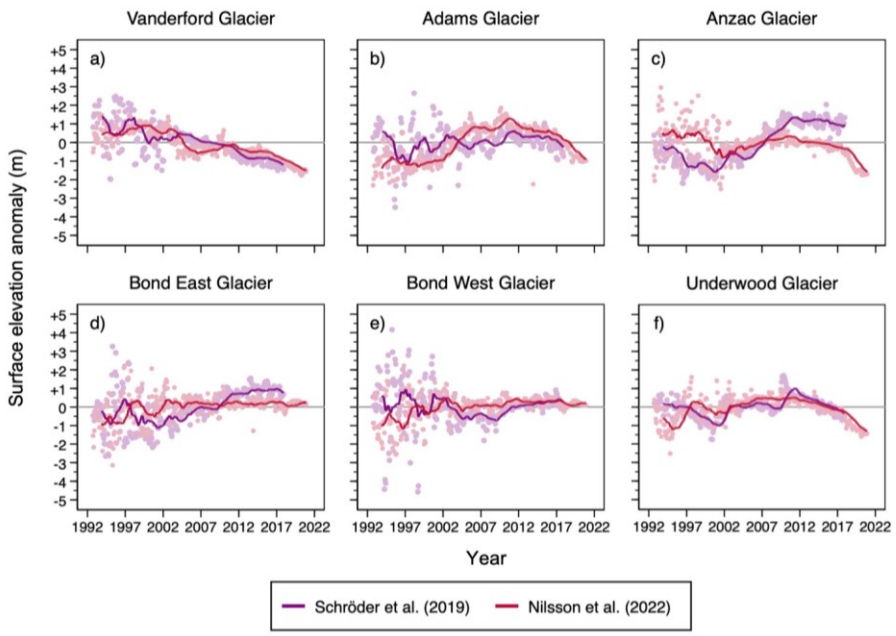

Figure 6. Monthly surface elevation anomalies observed in each GL box at (a) Vanderford Glacier, (b) Adams Glacier, (c) Anzac Glacier, (d) Bond East Glacier, (e) Bond West Glacier, and (f) Underwood Glacier between 1992 and 2020. Elevation anomalies are calculated relative to the long-term 1992-2017 mean. Bold lines represent 24-month rolling means.

Mirroring the elevation patterns observed by Schröder et al. (2019) and Nilsson et al. (2022), similar trends are found in the ICESat/ICESat-2-derived data of Smith et al. (2020) (Figure 7). Whilst Vanderford, Adams, Anzac and Underwood Glaciers showed an overall decrease in ice-surface elevation between 2003 and 2019, both the Bond East and Bond West Glaciers exhibited minor thickening across the same time period. Such minor thickening was concentrated within ~ 35 km of the coastline, with ice-surface elevation comparatively stable inland of the Bond East and Bond West flowlines (Figure 7).

Deleted: ice surface

Formatted: Font color: Auto

Formatted: Font color: Auto

Deleted: These trends in ice surface elevation change were also reflected in the dataset produced by

Deleted: ice surface

Deleted: ice surface

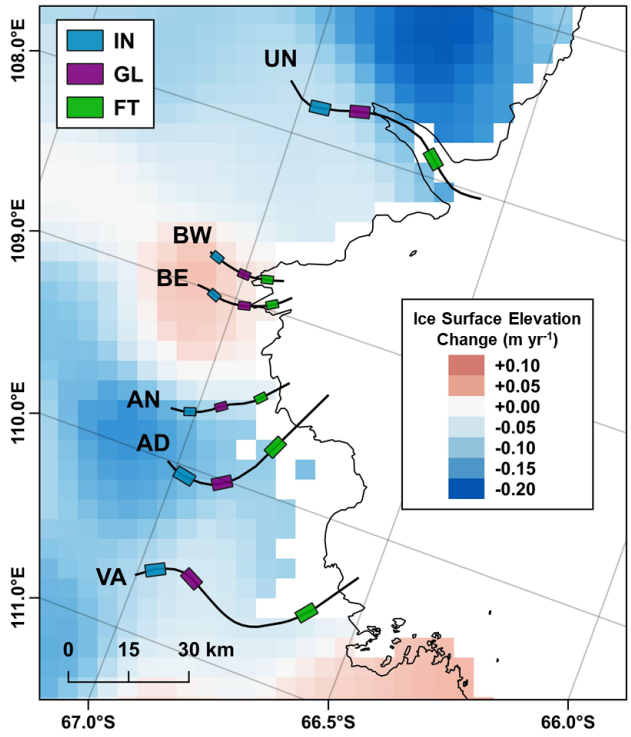

Figure 7. Rate of ice surface elevation change observed inland of Vincennes Bay between 2003 and 2019, as calculated by Smith et al. (2020). Coastline, shown in black, downloaded from the SCAR Antarctic Digital Database, accessed using Quantarctica 3 (Matsuoka et al., 2021).

3.4 Grounding-line Position

Vanderford Glacier showed the greatest and most consistent grounding-line retreat across the observational period, retreating ~ 18.6 km between 1996 and 2020, at an average rate of -0.8 km yr^{-1} (Figure 8a). This magnitude of retreat falls greatly outside the estimated error values provided with each dataset (Table 2), and likely exceeds any uncertainties associated with comparing the hinge-line (AIS CCI and MEaSUREs) and break-in-slope (ASAID and MOA). The rapid grounding-line retreat primarily occurred down a retrograde bedrock slope, however the most recent observed grounding-line position appears to be situated

Deleted:
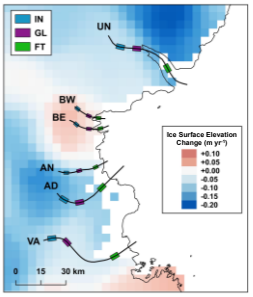

Formatted: Font color: Auto

Formatted: Font color: Auto

Deleted: ice surface

Deleted: Grounding Line

Deleted: grounding line

Deleted: Such

Deleted: grounding line

Deleted: but

Deleted: grounding line

on a stabilising ridge (Figure 9a). Between 2016 and 2020, the average rate of grounding-line retreat increased to 1.0 km yr^{-1}, with ~4.1 km of grounding-line retreat measured over this 4-year period (Figure 8a).

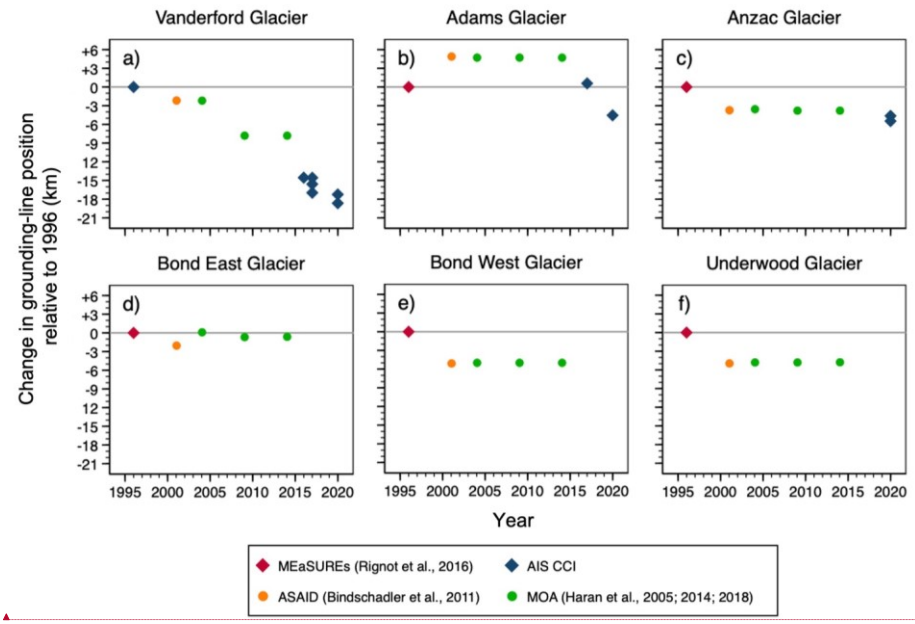

Figure 8. Change in grounding-line position measured relative to the minimum observed 1996 position at (a) Vanderford Glacier, (b) Adams Glacier, (c) Anzac Glacier, (d) Bond East Glacier, (e) Bond West Glacier, and (f) Underwood Glacier. Note that circles represent grounding-line positions derived from optical imagery, whilst diamonds represent grounding-line products derived using DInSAR.

Deleted: grounding line

Deleted: grounding line

Deleted: ¶

Formatted: Font color: Auto

Formatted: Font color: Auto

Deleted: grounding line

Deleted: grounding line

Deleted: manually

Deleted: grounding line

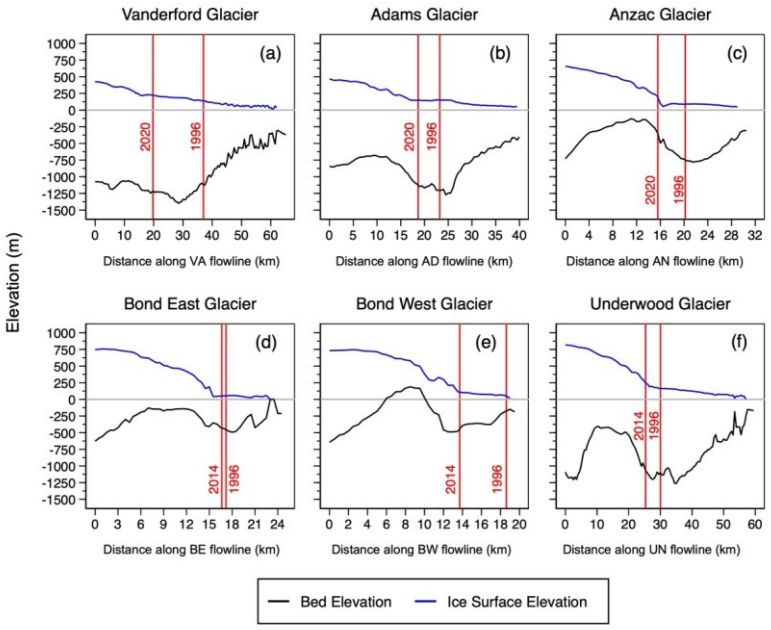

Figure 9. Ice surface (Howat et al., 2019) and bedrock elevation (Morlighem, 2020) profiles extracted along the central flowlines of (a) Vanderford Glacier, (b) Adams Glacier, (c) Anzac Glacier, (d) Bond East Glacier, (e) Bond West Glacier, and (f) Underwood Glacier. Dated vertical red lines represent the oldest and most recent grounding-line positions observed respectively. Note that distance is measured in the along-flow direction, with 0 km representing the inland start point of each respective flowline.

In contrast, the grounding-line positions of the Adams, Anzac, Bond East, Bond West, and Underwood Glaciers were observed to be stable between 2001 and 2014, with the ASAID and MOA grounding-line products digitised in nearly identical locations (Figure 8). Despite an initial grounding-line advance of ~ 5 km between 1996 and 2001, an overall retreat of ~ 4.5 km was observed at Adams Glacier between 1996 and 2020 (Figure 8b). A similar overall pattern of grounding-line retreat was observed at Anzac Glacier, measured at ~ 5.4 km over the same time period (Figure 8c).

Between 1996 and 2014, Bond West and Underwood Glacier exhibited very similar patterns of grounding-line retreat, retreating ~4.9 and ~4.7 km, respectively (Figure 8). The majority of this retreat was observed between 1996 and 2001. Unlike the other outlet glaciers within Vincennes Bay, Bond East's grounding-line was seen to be stable across the observational period (Figure 8d). Between 1996 and 2001, the grounding-line was estimated to have retreated ~2 km. However, between

Deleted:
Formatted: Font color: Auto
Formatted: Font color: Auto
Deleted: grounding line
Deleted: downstream
Formatted: Font color: Auto
Deleted: grounding line
Deleted: grounding line
Deleted: grounding line
Deleted: grounding line
Deleted: grounding line
Deleted: grounding line
Deleted: grounding line

2004 and 2014, Bond East's grounding-line remained within ~600 m of the observed 1996 position. It should be noted that more recent grounding-line positions were not available at the Bond East, Bond West, and Underwood Glaciers.

4. Discussion

4.1. Recent dynamic change and future evolution of Vanderford Glacier

Our results show a continuation of notable grounding-line retreat at Vanderford Glacier, measured at 18.6 km between 1996 and 2020 (Figure 8a). This represents an average rate of retreat of 0.78 km yr^{-1}, corresponding closely with the 17 km of grounding-line retreat previously observed by Rignot et al. (2019) between 1996 and 2017 (0.81 km yr^{-1}). This high rate of retreat places Vanderford Glacier as the fastest retreating glacier in East Antarctica over decadal time-scales (Konrad et al., 2018; Stokes et al., 2022). Only Thwaites and Pine Island Glacier have sustained higher rates of grounding-line retreat, measured at 0.8 km yr^{-1} (1992-2011) (Milillo et al., 2019) and 0.95 km yr^{-1} (1992-2011) (Park et al., 2013) respectively, over the satellite era. Such high rates of retreat have widely been attributed to the enhanced intrusion of warm mCDW across the continental shelf towards sub ice-shelf cavities (Thoma et al., 2008; Steig et al., 2012; Paolo et al., 2015; Turner et al., 2017a; Scambos et al., 2017; Rignot et al., 2019). The marked grounding-line retreat observed at Vanderford Glacier is therefore consistent with the notion that warm mCDW is able to access local ice-shelf cavities below the Vanderford Ice Shelf, driving high rates of basal melting (Depoorter et al., 2013; Ribeiro et al., 2021).

The rapid rate of grounding-line retreat measured at Vanderford Glacier is anomalous within Vincennes Bay, calculated to be nearly four times greater than the average rate of retreat (0.20 km yr^{-1}) recorded across the Adams, Anzac, Bond East, Bond West, and Underwood Glaciers. With mCDW typically observed to access sub ice-shelf cavities via deep subglacial troughs (Jenkins et al., 2010; Scambos et al., 2017; Rignot et al., 2019), this significant difference may be indicative of a bathymetric pathway that favours preferential intrusion of mCDW towards the Vanderford Ice Shelf, rather than the other studied glaciers. Bathymetric data remains limited across Vincennes Bay, but recent echosounding carried out onboard RSV *Nuyina* revealed an undiscovered canyon at the front of Vanderford Glacier, estimated to be more than 55 kilometres in length, reaching a maximum depth of 2200 m (Figure 10) (Australian Antarctic Division, 2022). This canyon provides a potential pathway for the incursion of mCDW at depth towards the Vanderford Ice Shelf, thereby facilitating enhanced rates of grounding-line retreat relative to the other Vincennes Bay outlet glaciers.

In addition, the anomalously high rate of grounding-line retreat observed at Vanderford Glacier may be attributed to the underlying bedrock geometry. Figure 9a indicates that between 1996 and 2020, the majority of Vanderford's grounding-line retreat occurred down a retrograde slope. In contrast, with the exception of Bond West Glacier (Figure 9e), the grounding-line retreat observed at other glaciers within Vincennes Bay generally occurred along prograde slopes. As retrograde bedrock slopes

Deleted: grounding line
Deleted: grounding line
Deleted: ¶
Deleted: extensive grounding linegrounding-line
Formatted: Font color: Auto
Deleted: corresponds to
Formatted: Font color: Auto
Formatted: Font color: Auto
Formatted: Font color: Auto
Formatted: Font color: Auto
Formatted: Font color: Auto
Formatted: Font color: Auto
Formatted: Font color: Auto
Formatted: Font color: Auto
Deleted: , representing the fastest decadal-scale grounding linegrounding-line retreat reported in East Antarctica (Stokes et al., 2022). Such retreat is consistent with that seen at Thwaites Glacier, measured at 0.8 km yr^{-1} between 1992 and 2017 (Milillo et al., 2019) and
Deleted: considered
Deleted: to result from
Deleted: grounding line
Formatted: Font color: Auto
Deleted: grounding line
Deleted: might
Formatted: Font color: Auto
Deleted: grounding line
Deleted: grounding line
Deleted: grounding line
Deleted: grounding line

favour more extensive grounding-line retreat for a given basal melt rate (Milillo et al., 2019; Millan et al., 2022), the high rate of grounding-line retreat seen at Vanderford Glacier may hence also be the product of the underlying bedrock geometry.

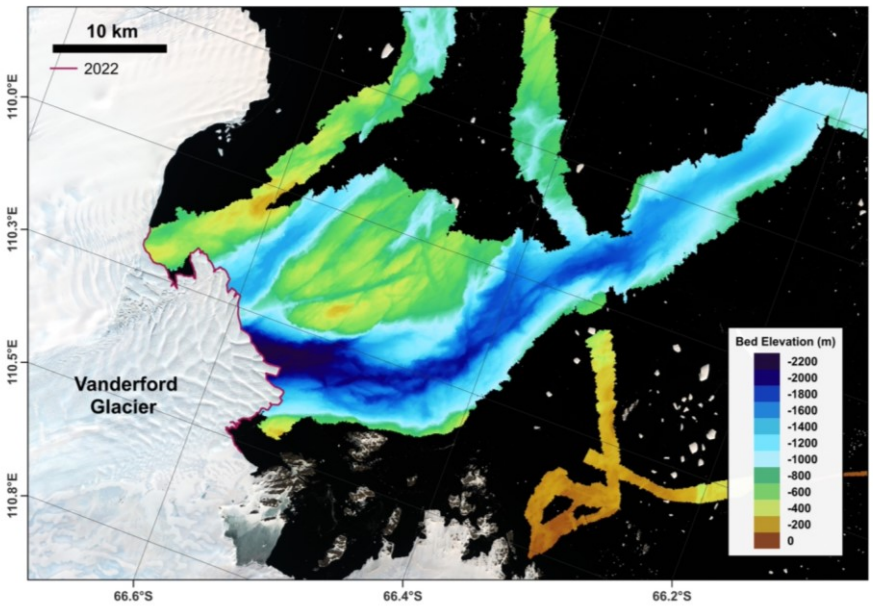

Figure 10. Bathymetry mapped at the front of Vanderford Glacier, collected during RSV *Nuyina's* maidan voyage to Antarctica (Commonwealth of Australia, 2022). Background satellite imagery was collected in February 2022, with red line showing the associated digitised terminus position.

The intrusion of warm mCDW to sub ice-shelf cavities facilitates enhanced oceanic thinning of floating ice shelves (Paolo et al., 2015). Such ice shelves transmit a critical buttressing force upstream, restraining the outflow of grounded ice (Fürst et al., 2016). The thinning of ice shelves reduces this buttressing potential, often triggering dynamic thinning and acceleration across upstream glaciers (Reese et al., 2018). For example, Thwaites Glacier accelerated by 33% between 2006 and 2013 (Mouginot et al., 2014), with dynamic thinning of at least 1.5 m yr^{-1} measured between 2012 and 2020 (Bevan et al., 2021). Whilst our results reveal a 31% increase in inland velocity at Vanderford Glacier between 2000 and 2013, velocity was seen to be stable across the grounding-line throughout the observational period (2000 – 2021), with no significant acceleration recorded (Figure 5a). In addition, although a consistent decrease in surface elevation was measured across Vanderford Glacier (Figure 6a), the average rate of ice thinning, calculated to range between -0.07 and -0.12 m yr^{-1} (2003 – 2017), was an order of magnitude

Deleted: grounding line

Deleted: grounding line

Deleted:

Formatted: Font color: Auto

Formatted: Font color: Auto

Deleted: the

Deleted: grounding line

lower than recorded at other glaciers undergoing similar rapid grounding-line retreat within the Amundsen Sea Embayment, such as Thwaites Glacier (Pritchard et al., 2009; Flament & Rémy, 2012; Konrad et al., 2017).

The lack of significant ice-surface elevation change across Vanderford Glacier could be attributed to variations in surface mass balance, with a comparatively high rate of snowfall within the Aurora subglacial basin potentially obscuring a dynamic thinning signal. However, the rate of surface lowering measured across the neighbouring Totten Glacier (Figure 1b) was also significantly higher than at Vanderford Glacier, estimated up to -1.7 m yr^{-1} between 2003 and 2008 (Khazendar et al., 2013). This suggests that the comparatively moderate rate of thinning seen across Vanderford Glacier is not the product of dynamic thinning being mitigated by high regional snowfall. Rather, the rate of dynamic thinning observed across Vanderford Glacier appears to have been significantly lower, indicating that the ocean-driven reduction in buttressing force exerted by the Vanderford Ice Shelf has presently been limited. This likely reflects that in Antarctica, the majority of basal melting is confined to the grounding zone, owing to both water column stratification and the role of pressure in determining the freezing point of seawater (Rignot et al., 2013). The relative lack of a dynamic response supports this notion, indicating that high basal melt rates have been concentrated at the grounding-line (Rignot et al., 2013), rather than across the Vanderford Ice Shelf.

Using remotely-sensed data and calculation of the volume flux divergence, Rignot et al. (2013) estimated area-averaged basal melt rates of 5.3 ± 2 m yr^{-1} under the Vincennes Bay ice-shelves. This is significantly lower than the area-averaged basal melt rates of the Thwaites and Pine Island ice-shelves, estimated at 17.7 ± 1 and 16.2 ± 1 m yr^{-1}, respectively (Rignot et al., 2013). However, accurate quantification of such basal melt rates remains challenging, particularly at the grounding-line. Direct point measurements can be obtained using radar instrumentation, such as the Autonomous Phase-sensitive Radio-Echo Sounder (ApRES) (Nicholls et al., 2015), but this requires in-situ deployment and remains uncertain across areas characterised by thick ice or by a high density of basal crevasses (Vaňková et al., 2021). Recent work has therefore favoured high-resolution remote-sensing methods in order to assess spatial variations in basal melt under individual ice-shelves (Berger et al., 2017; Shean et al., 2019). Future application of such methods could provide more accurate estimates of basal melt rates under the Vanderford Ice Shelf, thereby allowing an assessment as to whether basal melt is largely confined to the grounding-line, as hypothesised.

Whilst Vanderford Glacier is currently grounded on a stabilising bedrock ridge (Figure 9a), extension of the central flowline shows that retrograde slopes are observed inland along the Vanderford Trench, with a significant decrease in bedrock elevation seen approximately 70 km inland of the present grounding-line position (Figure 11c). If the current rate of grounding-line retreat (0.78 km yr^{-1}) was to continue, this steep bedrock slope would be reached within 100 years, potentially triggering MISI. Indeed, using the BISICLES adaptive mesh ice-sheet model, Sun et al. (2016) simulated Vanderford's grounding-line to retreat rapidly along the Vanderford Trench, separating Law Dome (Figure 1b) from the continental ice sheet within 1000 years. However, Sun et al. (2016) also emphasised that such extensive grounding-line retreat is dependent on the future oceanic forcing, requiring basal melt rates elevated above those observed at present.

Deleted: grounding line

Deleted: is

Formatted: Font color: Auto

Formatted: Font color: Auto

Formatted: Font color: Auto

Deleted: er

Deleted: therefore

Deleted: . This

Formatted: Font color: Auto

Deleted: es

Formatted: Font color: Auto

Formatted: Font color: Auto

Formatted: Font color: Auto

Deleted: Nonetheless, Fürst et al. (2016) calculated that just 20.2% of the Vanderford Ice Shelf is categorised as passive, i.e. can be removed without initiating a dynamic glaciological response. It may thus be predicted that continued intrusion of warm mCDW will likely reduce the buttressing force exerted by the Vanderford Ice Shelf, potentially initiating acceleration and enhanced dynamic thinning across Vanderford Glacier in the coming decades.¶

Deleted: grounding line

Deleted: grounding line

Deleted: grounding line

Deleted: grounding line

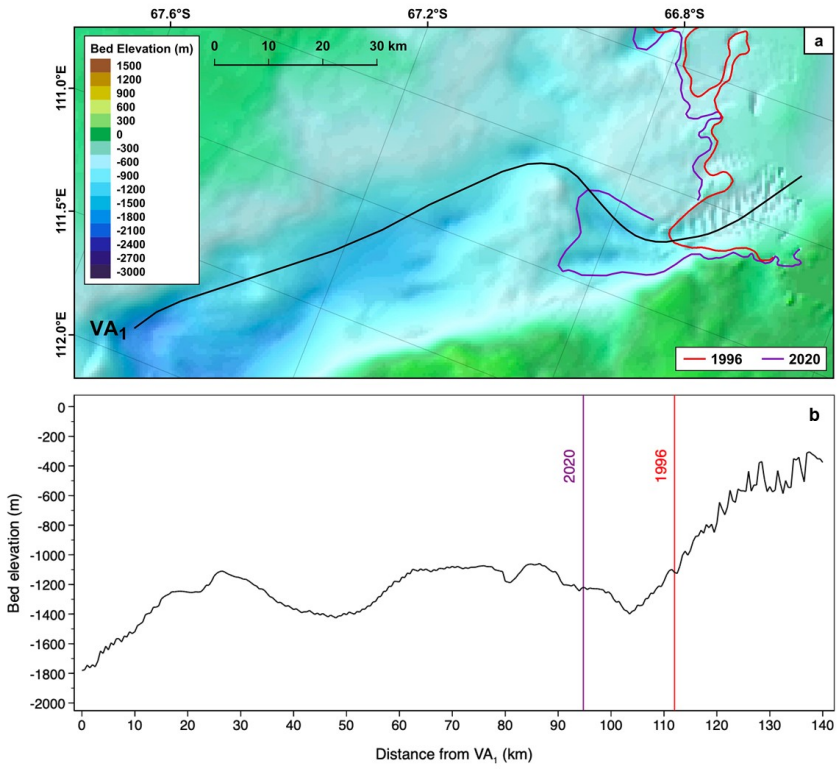

Figure 11. a) Location of an extended flowline digitised along the main flow of Vanderford Glacier. Background shows BedMachine bed elevation, underlain by a hillshade (Morlighem, 2020). b) Bed elevation sampled from BedMachine (Morlighem, 2020) along the extended flowline. 1996 MEaSUREs (Rignot et al., 2016) and 2020 AIS CCI grounding-line positions are displayed in red and purple respectively.

Recent oceanographic observations suggest that the oceanic heat supply to East Antarctica is increasing (Herraiz-Borreguero & Garabato, 2022), potentially facilitating increased basal melt rates. The mid-depth CDW found along the continental slope off East Antarctica has warmed significantly since the 1990s, with an increase of 0.29°C per decade estimated near Vincennes Bay (105 °E – 111°E). This warming has been attributed to the southward shift of the Antarctic Circumpolar Current (ACC)

Deleted: ¶

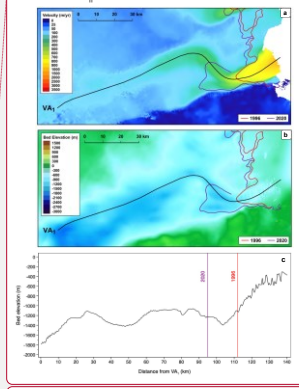

Formatted: Font color: Auto

Formatted: Font color: Auto

Formatted: Font color: Auto

Formatted: Font color: Auto

Deleted: E

Deleted: r

Deleted: overlain on maps of a) ice velocity extracted from the 2018 ITS_LIVE ice velocity mosaic (Gardner et al., 2022), and b) bedrock topography extracted from BedMachine (Morlighem, 2020). c) Bed elevation sampled from BedMachine (Morlighem, 2020) along the extended flowline.

Deleted: grounding line

Deleted: such

(Yamazaki et al., 2021), understood to have been driven by a poleward shift of the westerlies over the Southern Ocean associated with summertime positive trends in the southern annular mode (Herraiz-Borreguero & Garabato, 2022). With climatic models predicting that the southern annular mode will continue trending towards its positive phase under high-emission scenarios (Zheng et al., 2013; Lim et al., 2016; Lee et al., 2021), further CDW warming may be expected off East Antarctica, enabling enhanced basal melt rates (Herraiz-Borreguero & Garabato, 2022). Subsequent increased outflow of glacial meltwater will likely further hinder the formation of DSW in the Vanderford polynya, thereby facilitating the enhanced incursion of warm mCDW at depth (Ribeiro et al., 2021). This positive feedback could drive rapid grounding-line retreat at Vanderford Glacier, potentially providing the oceanic forcing required to initiate MISI (Sun et al., 2016). Such a mechanism may support recent modelling conducted by Jordan et al. (2023), contributing to the negative mass balance predicted across the EAIS in response to enhanced mCDW intrusion onto the continental shelf.

4.2. The role of sea-ice in controlling outlet glacier ice dynamics

Taken together, the decadal variations in terminus position observed across Vincennes Bay (Table 3) are seen to correspond closely with the wider decadal-scale patterns reported along the Wilkes Land coast (Miles et al., 2016) (Figure 12). The majority of Wilkes Land outlet glaciers were seen to retreat between 1974-1990, switch to a period of sustained advance between 1990-2000, before retreating again between 2000-2012 (Miles et al., 2016). Miles et al. (2016) suggest that such decadal fluctuations between terminus retreat and terminus advance are strongly correlated to rates of sea-ice production around East Antarctica, emphasising the role of sea-ice formation in modulating the intrusion of warm mCDW towards glacier termini. Miles et al. (2016) explain that increased sea-ice production enhances brine rejection and can lead to destratification of the water column (Petty et al., 2014), thereby facilitating the formation of DSW and production of Antarctic Bottom Water (AABW) (Kusahara et al., 2011). Such AABW represents the densest water mass in the ocean (Ribeiro et al., 2021) and therefore inhibits the intrusion of mCDW at depth, suppressing rates of basal melt and facilitating terminus advance (Miles et al., 2016). In contrast, decreased sea-ice production is understood to reduce the formation of DSW and the associated production of AABW, thereby allowing enhanced intrusion of mCDW at depth. Miles et al. (2016) conclude that such enhanced intrusion increases rates of basal melt, with negative sea-ice anomalies therefore attributed to the periods of synchronous terminus retreat observed along the Wilkes Land coast (1974-1990, 2000-2012; Figure 12) (Miles et al., 2016).

Deleted: grounding line

Deleted:

Formatted: Font color: Auto

Deleted: ¶

Formatted: Font color: Auto

Deleted: **Decadal patterns of terminus position change observed across the Vincennes Bay outlet glaciers potentially correlated to sea ice production**

Deleted: T

Formatted: Font color: Auto

Deleted: ed

Deleted: .

Deleted: They noted that enhanced brine rejection from increased sea-ice production can result in

Deleted: hence

Deleted: Representing the densest water mass in the ocean (Ribeiro et al., 2021), AABW is understood to inhibit intrusion of mCDW, thereby suppressing basal melting and

Deleted: leads to a reduction in DSW formation

Deleted: and hence decreased production of AABW. This allows enhanced intrusion of mCDW, driving basal melting and thus terminus retreat (Miles et al., 2016). Whilst detailed analysis of decadal trends in sea ice production is yet to be carried out within Vincennes Bay, Miles et al. (2016) noted a negative correlation between sea-ice production and average air temperatures over the sea-ice production season (April to October) along the Wilkes Land coast. ¶

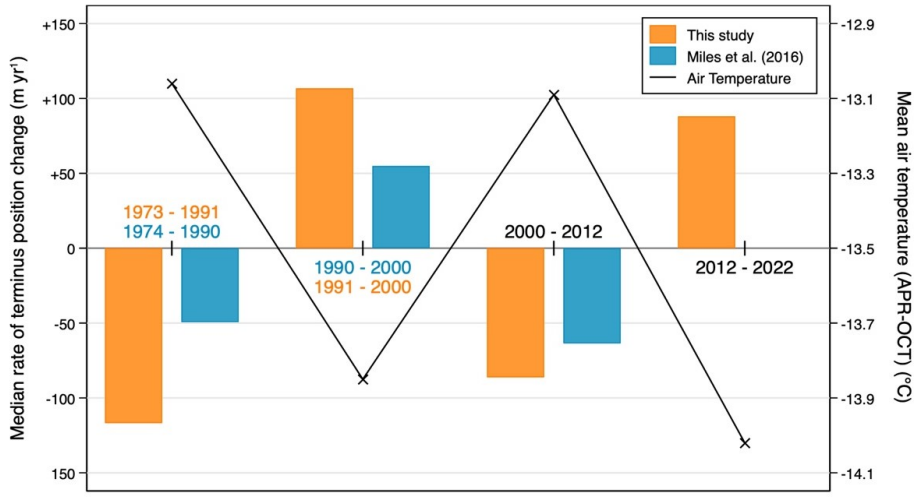

Figure 12. Median decadal terminus position change reported in this study within Vincennes Bay, shown in orange, in comparison to that observed along the Wilkes Land coastline by Miles et al. (2016), shown in blue. This study (n = 6), Miles et al. (2016) (n= 15 (1974-1990), 37 (1990-2000), 39 (2000-2012)). Mean surface air temperatures measured at Casey Station (66.3°S 110.5°E) over the sea-ice production season (April to October), extracted from Met-READER (2022), displayed in black.

However, as discussed previously, the majority of basal melting is confined to the grounding zone in Antarctica (Rignot et al., 2013). It is perhaps therefore more likely that variations in sea-ice coverage influenced outlet glacier terminus positions within Vincennes Bay by modulating the buttressing provided. Landfast sea-ice and mélange exerts a resistive backstress at the ice-front, reducing the frequency of calving events and increasing terminus stability (Amundson et al., 2010; Gomez-Fell et al., 2022). Previous calving and ice-shelf disaggregation events observed in Wilkes Land have therefore been linked to the break-up of multi-year landfast sea-ice (Miles et al., 2017), and removal of mélange from the ice-front (Arthur et al., 2021). Recent work has also emphasised the important role that sea-ice appears to play in protecting coastal regions from storm-generated ocean swells, with reduced sea-ice concentrations associated with steep sea-surface slopes observed to initiate calving (Massom et al., 2018; Francis et al., 2021; Christie et al., 2022). Whilst the relative importance of each mechanism remains unclear within Vincennes Bay, it is apparent that sea-ice may play a critical role in determining the frontal position of the studied outlet glaciers.

Formatted: Font color: Auto
Formatted: Font color: Auto
Deleted:
Formatted: Font color: Auto
Formatted: Font color: Auto

A detailed analysis of decadal trends in sea-ice production is yet to be carried out within Vincennes Bay, however Miles et al. (2016) have previously noted a negative correlation between sea-ice production and average air temperatures over the sea-ice production season (April to October) along the Wilkes Land coast. To consider this potential correlation, monthly surface air temperature data collected at Casey Station (Figure 1b) were downloaded and analysed (Met-READER, 2022). The results indicate that such a negative correlation was also observed within Vincennes Bay, with higher temperatures, and thus reduced sea-ice concentrations by proxy, observed to be coincident with periods of terminus retreat (Figure 12). The decrease in mean surface air temperature and overall pattern of terminus advance observed between 2012-2022 (Figure 12) may therefore be indicative of increased sea-ice production within Vincennes Bay over this most recent decade.

Nonetheless, analysis of ice-surface elevation shows a pattern of accelerated thinning across each of the Vanderford, Adams, Anzac, and Underwood Glaciers between 2017 and 2020 (Figure 6). The most significant acceleration was measured at Anzac Glacier, with the average rate of thinning increasing from -0.01 m yr^{-1} between 2003 and 2017 to -0.44 m yr^{-1} between 2017 and 2020 (Table 4) (Nilsson et al., 2022). Whilst the observational period is relatively short, this synchronous dynamic response is potentially indicative of a common external forcing and a minimal lag-time. One such forcing may have been the significant decline in Antarctic sea-ice extent seen during the austral spring of 2016 (Turner et al., 2017b). Although negative sea-ice anomalies were observed to be transient across the Western Pacific Ocean (90°E – 160°E) (Turner et al., 2017b), decreased production of sea-ice may have driven increased rates of basal melt (Miles et al., 2016) and reduced the resistive backstress exerted at the ice-front (Amundson et al., 2010; Gomez-Fell et al., 2022). With each of the Vanderford, Adams, and Underwood glaciers undergoing a period of sustained terminus advance between 2017 and 2020 (Figure 2), such reduced buttressing appears to have facilitated longitudinal thinning across the grounding-line. The reduced stability of the glacier termini (Admundson et al., 2010) may have also contributed to the spectacular disintegration of Underwood's floating tongue observed between 2020 and 2022 (Figure 2f). With a satellite-era record minimum Antarctic sea-ice extent observed in February 2022 (Turner et al., 2022), Vanderford Glacier could be expected to experience a similar significant calving event in the immediate future. However, more detailed analysis of sea-ice variability within Vincennes Bay is required in order to better understand these potentially important ice-ocean interactions.

Average rate of thinning (m yr^{-1})

	Vanderford	Adams	Anzac	Underwood
2003 - 2017	-0.07	-0.02	-0.01	-0.03
2017 – 2020	-0.22	-0.32	-0.44	-0.38

Table 4. The average rate of thinning observed within the GL box of the Vanderford, Adams, Anzac, and Underwood Glaciers between 2003-2017 and 2017-2020, respectively. Note that these rates of thinning were extracted from the ice-surface elevation dataset provided by Nilsson et al. (2022).

Deleted: within Vincennes Bay

Deleted: d

Deleted: , with higher temperatures

Deleted:

Moved (insertion) [1]

Deleted: A

Deleted: ice surface

Formatted: Font color: Auto, Superscript

Formatted: Font color: Auto

Formatted: Font color: Auto, Superscript

Formatted: Font color: Auto

Formatted: Font color: Auto

Formatted: Font color: Auto

Deleted:

Deleted: seen

Formatted: Font color: Auto

Deleted: ¶
4.3. Enhanced thinning of the Vanderford, Adams, Anzac, and Underwood Glaciers observed between 2017 and 2020¶

Moved up [1]: Analysis of ice surface elevation shows a pattern of accelerated thinning across each of the Vanderford, Adams, Anzac, and Underwood Glaciers between 2017 and 2020 (Figure 6). The most significant acceleration was measured at Anzac Glacier, with the average rate of thinning increasing from -0.01 m yr^{-1} between 2003 and 2017 to -0.44 m yr^{-1} between 2017 and 2020 (Table 4) (Nilsson et al., 2022). ¶

Formatted: Font color: Auto

Formatted: Font color: Auto

Deleted: ice surface

4.3. High velocity at Bond West Glacier

Ice discharge across the grounding-line is dependent on ice velocity (Moon et al., 2015); the accurate assessment of ice velocity is hence crucial for determining sea level contributions. In comparison to the other outlet glaciers within Vincennes Bay, Bond West Glacier flows at a significantly higher velocity (Figure 4). The fastest flowing outlet glacier in East Antarctica, Shirase Glacier, is measured to reach speeds in excess of 2,200 m yr^{-1} across the grounding-line (Miles et al. 2022), with a maximum speed of 2,700 m yr^{-1} measured at the calving front (Pattyn & Derauw, 2002). Whilst Bond West flows more slowly across its grounding-line, at an average velocity of 1,463 m yr^{-1} (2002 – 2021), a more extreme acceleration is observed across Bond West's floating tongue, with a maximum flow speed of 3,344 m yr^{-1} measured in 2002 (Figure 5e). The floating tongue is thus heavily fractured (Figure 3e), showing a crevasse pattern more typically observed across fast-moving Greenlandic glaciers, such as Jakobshavn Isbræ (Mayer & Herzfeld, 2000). The high ice-surface velocity measured across Bond West's floating tongue may be a product of the underlying bedrock topography, with a steep slope of 9.6° measured immediately upstream of the grounding-line (Figure 9e). In addition, fast-flowing upstream ice is observed to converge through a comparatively narrow ice-shelf, constrained to the east by a stable ice rise and to the west by elevated bedrock topography (Figure 1b). Enhanced ice velocity must thus occur in order to maintain constant ice discharge through a smaller cross-sectional area (Winsborrow et al., 2010).

4.4. Importance of accurate DInSAR grounding-line mapping

The accurate mapping of grounding-line positions is fundamental for understanding ice sheet mass balance and assessing potential future contributions to sea level rise (Rignot et al., 2014; Mohajerani et al., 2021). However, Antarctic grounding-line positions have been mapped using a variety of different methods, with the term 'grounding line' often being used to refer to different distinct features across the grounding zone (Bindschadler et al., 2011). The most accurate mapping technique is typically considered to be DInSAR, with the hinge-line being used as a proxy for the grounding line, derived precisely through the analysis of tidally induced vertical motion (Rignot et al., 2014; Li et al., 2021; Mohajerani et al., 2021). In contrast, the manual digitisation of grounding-line positions from optical imagery, delineated using the most seaward observed break-in-slope, can be associated with high levels of uncertainty (Fricker et al., 2009; Rignot et al., 2011), particularly at fast-flowing outlet glaciers such as those found within Vincennes Bay (Bindschadler et al., 2011; Christie et al., 2016). This has been attributed to the notion that fast-flowing ice streams are typically moving via basal sliding, meaning the transition to zero basal resistance across the ice-shelf therefore produces a less marked break-in-slope (Rignot et al., 2011). With the exception of Vanderford Glacier, the results presented in this study show that the grounding-line positions mapped from optical imagery (ASAID and MOA datasets) are located in near-identical locations at each of the Vincennes Bay outlet glaciers between 2001

Deleted: Whilst the observational period is relatively short, this synchronous dynamic response may potentially be indicative of a common external forcing. With the negative correlation between sea ice production and the intrusion of mCDW previously outlined (Miles et al., 2016), such enhanced thinning could be related to the Whilst negative sea ice anomalies were observed to be transient across the Western Pacific Ocean (90°E – 160°E) (Turner et al., 2017b), decreased production of sea ice may have facilitated the increased incursion of warm mCDW within Vincennes Bay, thereby driving enhanced basal melting and dynamic thinning across the studied outlet glaciers. With a satellite-era record minimum Antarctic sea ice extent observed in February 2022 (Turner et al., 2022), such accelerated thinning may be expected to continue in the immediate future.¶

¶

In addition, the significant decline in Antarctic sea ice extent observed in 2016 (Turner et al., 2017b) may have had potentially important implications for the stability of the glacier termini. Previous analysis of outlet glacier dynamics within Porpoise Bay revealed that large calving events observed in January 2007 and March 2016 were linked to the break-up of multi-year landfast sea ice (Miles et al., 2017). Miles et al. (2017) therefore emphasised that sea ice concentrations can exert a significant control on terminus stability, supporting correlations between terminus change and sea ice mélange conditions previously observed in Greenland (Reeh et al., 2001; Moon et al., 2015). The negative sea ice anomalies seen in 2016 (Turner et al., 2017b) may thus have reduced the stability of the outlet glacier termini, facilitating terminus advance and associated longitudinal thinning across the grounding linegrounding-line. Indeed, analysis of terminus position change indicates that each of the Vanderford, Adams, and Underwood glaciers underwent a period of sustained advance between 2017 and 2020 (Figure 2). However, Anzac Glacier was recorded to be comparatively stable between 2017 and 2020, retreating by just -86 m (Figure 2). This suggests the enhanced rate of thinning measured across Anzac Glacier was not the product of longitudinal thinning. It may thus be inferred that the thinning instead occurred in situ, perhaps further supporting the ...

Deleted: 4

Deleted: grounding line

Deleted: grounding line

Deleted: grounding line

Deleted: ice surface

Deleted: grounding line

Deleted:

Deleted: 5

Deleted: **grounding line**

Deleted: grounding line

Deleted: grounding line

Deleted: grounding line

Deleted: grounding-line positions

Deleted: grounding line

Deleted:

Deleted: grounding line

and 2014 (Figure 8). Whilst this may be indicative of grounding-line stability, the lack of precise DInSAR grounding-line mapping over this time period precludes such inferences being made with certainty. We therefore propose that such DInSAR techniques should be prioritised in order to facilitate accurate grounding-line mapping across such potentially dynamic regions of East Antarctica.

5. Conclusions

This study provides the first detailed investigation of ice dynamics observed across the outlet glaciers of Vincennes Bay, a region recently recorded to have the warmest intrusions of mCDW within East Antarctica (Ribeiro et al., 2021). We observe a continuation of extensive grounding-line retreat at Vanderford Glacier (cf. Rignot et al., 2019), measured at 18.6 km between 1996 and 2020. This represents an average rate of retreat of 0.78 km yr^{-1} and corresponds closely with the 17 km of grounding-line retreat previously observed by Rignot et al. (2019) between 1996 and 2017 (0.81 km yr^{-1}). It also places Vanderford Glacier as the fastest retreating glacier in East Antarctica (Konrad et al., 2018; Stokes et al., 2022), and the third fastest retreating glacier across the Antarctic Ice Sheet, at the decadal scale. Such rapid retreat is consistent with the notion that warm mCDW is able to intrude at depth, accessing cavities formed below the Vanderford Ice Shelf (Depoorter et al., 2013; Ribeiro et al., 2021). With the long-term rate of ice-surface elevation change observed to be relatively minimal across Vanderford Glacier, such mCDW appears to be intruding to the grounding zone, driving high rates of basal melting at the grounding-line (Rignot et al., 2013), rather than across the Vanderford Ice Shelf. Whilst currently grounded on a stabilising bedrock ridge, retrograde slopes are observed inland along the Vanderford Trench. If grounding-line retreat continues at the present rate, this retrograde slope will be reached within 100 years, raising the potential for MISI. With basal melt predicted to further inhibit the formation of DSW within the Vanderford polynya (Ribeiro et al., 2021; Herraiz-Borreguero & Garabato, 2022), mCDW intrusion may be enhanced, thereby providing the oceanic forcing required to drive further grounding-line retreat.

In comparison to Vanderford Glacier, the extent of grounding-line retreat observed across the Adams, Anzac, Bond East, Bond West, and Underwood Glaciers was significantly lower, averaged at a rate of 0.2 km yr^{-1}. With a recently discovered canyon providing a potential bathymetric pathway for mCDW intrusion towards Vanderford Glacier, the comparatively lower rates of grounding-line retreat observed across the remaining Vincennes Bay outlet glaciers may be indicative of a relative lack of bathymetric pathways towards these termini. Indeed, the grounding-line positions of the Adams, Anzac, Bond East, Bond West, and Underwood Glaciers were seen to be stable between 2001 and 2014. However, such stability was inferred from datasets derived through manual digitisation of the most seaward observed break-in-slope and are hence associated with higher levels of uncertainty. The results of this study thus emphasise the need to prioritise precise mapping of grounding-line positions using DInSAR techniques, particularly across dynamic regions, such as Wilkes Land.

Deleted: grounding line
Deleted: grounding line
Deleted: grounding line
Deleted: Our results confirm
Formatted: Font color: Auto
Deleted: grounding line
Formatted: Font color: Auto
Deleted: , representing an average retreat rate of 0.8 km yr^{-1}.
Deleted:
Formatted: Font color: Auto
Formatted: Font color: Auto
Deleted: This reflects the highest rate of grounding linegrounding-line retreat reported for any glacier within East Antarctica and is consistent
Deleted: and driving high rates of basal melt (Depoorter et al., 2013; Ribeiro et al., 2021).
Formatted: Font color: Auto
Deleted: grounding line
Deleted: grounding line
Deleted: .
Formatted: Font color: Auto

This study also reveals that decadal changes in frontal position measured across the Vincennes Bay outlet glaciers correspond closely with wider patterns reported along the Wilkes Land coastline (Miles et al., 2016). Analysis of air surface temperature data collected at Casey Station supports the notion that such trends may be related to variations in sea-ice production. Negative sea-ice anomalies are discussed to drive terminus retreat through three primary mechanisms: (i) limiting the formation of DSW and thus facilitating enhanced intrusion of mCDW at depth (Miles et al., 2016), (ii) reducing the backstress exerted on the ice-front, thereby decreasing terminus stability (Amundson et al., 2010), and (iii) increasing the vulnerability of the ice-front to storm-generated ocean swells (Massom et al., 2018; Francis et al., 2021; Christie et al., 2022). The role of sea-ice debuttressing and enhanced mCDW intrusion is also attributed to the accelerated thinning observed across each of the Vanderford, Adams, Anzac, and Underwood Glaciers between 2017 and 2020, facilitating longitudinal thinning across the grounding-line. Further analysis of sea-ice variability and such potentially important ice-ocean interactions is therefore required in order to better understand outlet glacier ice dynamics within Vincennes Bay.

6. Data Availability

The Landsat and Sentinel imagery used in this study are available from the United States Geological Survey EarthExplorer (https://earthexplorer.usgs.gov/). The manually digitised terminus positions, central flowlines and sampling boxes are available to download from the UK Polar Data Centre (https://doi.org/10.5285/4D4BD383-F6BB-4476-9058-D883B7706B26). The ITS_LIVE annual velocity mosaics (2000-2018) are available from NASA's National Snow and Ice Data Center (NSIDC) (https://doi.org/10.5067/6II6VW8LLWJ7), whilst the ENVEO monthly velocity mosaics (2018-2020) are available from the NERC EDS Centre for Environmental Data Analysis (http://dx.doi.org/10.5285/00fe090efc58446e8980992a617f632f). The monthly surface elevation change datasets produced by Schröder et al. (2019) (1978-2017) and Nilsson et al. (2022) (1985-2020) are available from (https://doi.org/10.1594/PANGAEA.897390) and (https://doi.org/10.5067/L3LSVDZS15ZV). The ice-column thickness-change-rate estimates (2003-2019) made by Smith et al. (2020) are available from the ResearchWorks Archive (http://hdl.handle.net/1773/45388). The AIS CCI grounding-line positions derived in this study are available from the ENVEO cryoportal (cryoportal.enveo.at), entitled 'GLL, Vincennes Bay, Antarctica, 1996 – 2020'. The MEaSUREs (Rignot et al., 2016) 1996 grounding-line positions are available from NASA's NSIDC (https://doi.org/10.5067/IKBWW4RYHF1Q). The MOA grounding-line positions from 2004 (Haran et al., 2005), 2009 (Haran et al., 2014), and 2014 (Haran et al., 2018) are also available from the NSIDC at (https://doi.org/10.5067/68TBT0CGJSOJ), (https://doi.org/10.5067/4ZL43A4619AF), and (https://doi.org/10.5067/RNF17BP824UM), respectively. The ASAID grounding-line dataset (1999-2003) is available from the U.S. Antarctic Program Data Center (http://dx.doi.org/10.7265/N56T0JK2). The monthly surface air temperature collected from Casey Station is available from (https://legacy.bas.ac.uk/met/READER/surface/Casey.All.temperature.html).

Deleted: Although the dynamic response of Vanderford Glacier
Formatted
Deleted: correlated …elated to variable sea ice
Formatted
Field Code Changed
Formatted
Deleted: are available upon request.
Field Code Changed
Formatted
Field Code Changed
Formatted
Field Code Changed
Formatted
Field Code Changed
Formatted
Field Code Changed
Formatted
Field Code Changed
Formatted
Deleted: grounding line
Deleted: .
Deleted: grounding line
Deleted: at
Field Code Changed
Formatted
Deleted: grounding line
Deleted: NASA's
Formatted
Deleted: at
Formatted
Formatted
Field Code Changed
Formatted
Field Code Changed
Field Code Changed
Formatted
Deleted: grounding line
Field Code Changed
Formatted
Field Code Changed
Formatted

7. Supplement

The supplement related to this article is available online at:

8. Author Contributions

HP, CS, and SJ designed the initial study. HP undertook the data collection and conducted the analysis, with guidance from CS and SJ. DF and LK completed the DInSAR grounding-line mapping within Vincennes Bay, with LK writing the associated methods section. HP led the remaining manuscript writing, with input and edits from all authors.

9. Competing Interests

CRS is a member of the editorial board of *The Cryosphere*.

10. Acknowledgements

CRS and SSRJ acknowledge funding from the Natural Environment Research Council (NE/R000824/1). The authors would also like to thank the Editor (Huw Horgan), Wei Ji Leong and an anonymous reviewer for their constructive comments on this manuscript.

References

Amundson, J., Fahnestock, M., Truffer, M., Brown, J., Lüthi, M., Motyka, R.: Ice mélange dynamics and implications for terminus stability, Jakobshavn Isbræ, Greenland, Journal of Geophysical Research, 115, F01005, https://doi.org/10.1029/2009JF001405, 2010.

Arthur, J., Stokes, C., Jamieson, S., Miles, B., Carr, R., Leeson, A.: The triggers of the disaggregation of Voyeykov Ice Shelf (2007), Wilkes Land, East Antarctica, and its subsequent evolution, Journal of Glaciology, 67, 265, 933-951, https://doi.org/10.1017/jog.2021.45, 2021.

Australian Antarctic Division: https://www.antarctica.gov.au/nuyina/stories/2022/rsv-nuyina-discovers-deep-glacial-canyon/, last access: 21 January 2022.

Berger, S., Drews, R., Helm, V., Sun, S., Pattyn, F.: Detecting high spatial variability of ice shelf basal mass balance, Roi Baudouin Ice Shelf, Antarctica, The Cryosphere, 11, 2675–2690, https://doi.org/10.5194/tc-11-2675-2017, 2017.

Formatted: Font color: Auto

Formatted: Normal

Deleted: grounding line

Formatted: Font color: Auto

Formatted: Font color: Auto

Moved down [2]: Australian Antarctic Division: https://www.antarctica.gov.au/nuyina/stories/2022/rsv-nuyina-discovers-deep-glacial-canyon/, last access: 21 January 2022.

Formatted: Font color: Auto

Formatted: Font color: Auto

Moved (insertion) [2]

Formatted: Font: Not Bold

Bevan, S. L., Luckman, A. J., Benn, D. I., Adusumilli, S., and Crawford, A.: Brief Communication: Thwaites Glacier cavity evolution, The Cryosphere, 15, 3317–3328, https://doi.org/10.5194/tc-15-3317-2021, 2021.

Bindschadler, R., Choi, H., Wichlacz, A., Bingham, R., Bohlander, J., Brunt, K., Corr, H., Drews, R., Fricker, H., Hall, M., Hindmarsh, R., Kohler, J., Padman, L., Rack, W., Rotschky, G., Urbini, S., Vornberger, P., and Young, N.: Getting around Antarctica: new high-resolution mappings of the grounded and freely-floating boundaries of the Antarctic ice sheet created for the International Polar Year, The Cryosphere, 5, 569–588, https://doi.org/10.5194/tc-5-569-2011, 2011.

Black, T. E. and Joughin, I.: Multi-decadal retreat of marine-terminating outlet glaciers in northwest and central-west Greenland, The Cryosphere, 16, 807–824, https://doi.org/10.5194/tc-16-807-2022, 2022.

Chen, X., Shearer, P. M., Walter, F., and Fricker, H. A.: Seventeen Antarctic seismic events detected by global surface waves and a possible link to calving events from satellite images, Journal of Geophysical Research: Solid Earth, 116, 1-16, https://doi.org/10.1029/2011JB008262, 2011.

Christianson, K., Bushuk, M., Dutrieux, P., Parizek, B. R., Joughin, I. R., Alley, R. B., Shean, D. E., Abrahamsen, E. P., Anandakrishnan, S., Heywood, K. J., Kim, T.-W., Lee, S. H., Nicholls, K., Stanton, T., Truffer, M., Webber, B. G. M., Jenkins, A., Jacobs, S., Bindschadler, R., and Holland, D. M.: Sensitivity of Pine Island Glacier to observed ocean forcing: PIG response to ocean forcing, Geophysical Research Letters, 43, 10,817-10,825, https://doi.org/10.1002/2016GL070500, 2016.

Christie, F. D. W., Bingham, R. G., Gourmelen, N., Tett, S. F. B., and Muto, A.: Four-decade record of pervasive grounding line retreat along the Bellingshausen margin of West Antarctica, Geophysical Research Letters, 43, 5741–5749, https://doi.org/10.1002/2016GL068972, 2016.

Christie, F. D. W., Benham, T., Batchelor, C., Rack, W., Montelli, A., Dowdeswell, J.: Antarctic ice-shelf advance driven by anomalous atmospheric and sea-ice circulation, Nature Geoscience, 15, 356-362, https://doi.org/10.1038/s41561-022-00938-x, 2022.

Commonwealth of Australia: RSV Nuyina Voyage 2 2021-22 Voyage Data, Southern Ocean, Antarctica, Version 1. Australian Antarctic Data Centre [data set], http://dx.doi.org/doi:10.26179/zz6j-e834, 2022.

Davis, E. R., Jones, D. J., Morgan, V. I., and Young, N. W.: A Survey of the Vanderford and Adams Glaciers in East Antarctica (Abstract), Annals of Glaciology, 8, 197–197, https://doi.org/10.3189/S0260305500001476, 1986.

Deleted: y

Formatted: Font color: Auto

Field Code Changed

Formatted: Font color: Auto

Formatted: Font color: Auto

Depoorter, M. A., Bamber, J. L., Griggs, J. A., Lenaerts, J. T. M., Ligtenberg, S. R. M., van den Broeke, M. R., and Moholdt, G.: Calving fluxes and basal melt rates of Antarctic ice shelves, Nature, 502, 89–92, https://doi.org/10.1038/nature12567, 2013.

ENVEO.: ESA Antarctic Ice Sheet Climate Change Initiative (Antarctic_Ice_Sheet_cci): Antarctic Ice Sheet monthly velocity from 2017 to 2020, derived from Sentinel-1, v1. NERC EDS Centre for Environmental Data Analysis [data set], http://dx.doi.org/10.5285/00fe090efc58446e8980992a617f632f, 2021.

Favier, L., Durand, G., Cornford, S. L., Gudmundsson, G. H., Gagliardini, O., Gillet-Chaulet, F., Zwinger, T., Payne, A. J., and Le Brocq, A. M.: Retreat of Pine Island Glacier controlled by marine ice-sheet instability, Nature Climate Change, 4, 117–121, https://doi.org/10.1038/nclimate2094, 2014.

Feldmann, J. and Levermann, A.: Collapse of the West Antarctic Ice Sheet after local destabilization of the Amundsen Basin, Proceedings of the National Academy of Sciences, 112, 14191–14196, https://doi.org/10.1073/pnas.1512482112, 2015.

Flament, T. and Rémy, F.: Dynamic thinning of Antarctic glaciers from along-track repeat radar altimetry, Journal of Glaciology, 58, 830–840, https://doi.org/10.3189/2012JoG11J118, 2012.

Francis, D., Mattingly, K., Lhermitte, S., Temimi, M., Heil, P.: Atmospheric extremes caused high oceanward sea surface slope triggering the biggest calving event in more than 50 years at the Amery Ice Shelf, 15, 2147-2165, https://doi.org/10.5194/tc-15-2147-2021, 2021.

Fricker, H. A., Coleman, R., Padman, L., Scambos, T. A., Bohlander, J., and Brunt, K. M.: Mapping the grounding zone of the Amery Ice Shelf, East Antarctica using InSAR, MODIS and ICESat, Antarctic Science, 21, 515–532, https://doi.org/10.1017/S095410200999023X, 2009.

Friedl, P., Weiser, F., Fluhrer, A., Braun, M.: Remote sensing of glacier and ice sheet grounding lines: A review, Earth-Science Reviews, 201, 102948, https://doi.org/10.1016/j.earscirev.2019.102948, 2020.

Fürst, J. J., Durand, G., Gillet-Chaulet, F., Tavard, L., Rankl, M., Braun, M., and Gagliardini, O.: The safety band of Antarctic ice shelves, Nature Climate Change, 6, 479–482, https://doi.org/10.1038/nclimate2912, 2016.

Gardner, A. S., Moholdt, G., Scambos, T., Fahnstock, M., Ligtenberg, S., van den Broeke, M., and Nilsson, J.: Increased West Antarctic and unchanged East Antarctic ice discharge over the last 7 years, The Cryosphere, 12, 521–547, https://doi.org/10.5194/tc-12-521-2018, 2018.

Field Code Changed
Formatted: Font color: Auto
Formatted: Font color: Auto
Formatted: Font color: Auto

Gardner, A., Fahnestock, M., Scambos, T.: ITS_LIVE Regional Glacier and Ice Sheet Surface Velocities: Version 1. National Snow and Ice Data Center [data set], https://doi.org/10.5067/6II6VW8LLWJ7, 2022.

Glasser, N. F., Scambos, T. A., Bohlander, J., Truffer, M., Pettit, E., and Davies, B. J.: From ice-shelf tributary to tidewater glacier: continued rapid recession, acceleration and thinning of Röhss Glacier following the 1995 collapse of the Prince Gustav Ice Shelf, Antarctic Peninsula, Journal of Glaciology, 57, 397–406, https://doi.org/10.3189/002214311796905578, 2011.

Goldstein, R. M., Engelhardt, H., Kamb, B., and Frolich, R. M.: Satellite Radar Interferometry for Monitoring Ice Sheet Motion: Application to an Antarctic Ice Stream, Science, 262, 1525–1530, https://doi.org/10.1126/science.262.5139.1525, 1993.

Gomez-Fell, R., Rack, W., Purdie, H., Marsh, O.: Parker Ice Tongue collapse, Antarctica, triggered by loss of stabilizing land-fast sea ice. Geophysical Research Letters, 49, e2021GL096156, https://doi.org/10.1029/2021GL096156, 2022.

Greenbaum, J. S., Blankenship, D. D., Young, D. A., Richter, T. G., Roberts, J. L., Aitken, A. R. A., Legresy, B., Schroeder, D. M., Warner, R. C., van Ommen, T. D., and Siegert, M. J.: Ocean access to a cavity beneath Totten Glacier in East Antarctica, Nature Geoscience, 8, 294–298, https://doi.org/10.1038/ngeo2388, 2015.

Greene, C. A., Blankenship, D. D., Gwyther, D. E., Silvano, A., and van Wijk, E.: Wind causes Totten Ice Shelf melt and acceleration, Science Advances, 3, e1701681, https://doi.org/10.1126/sciadv.1701681, 2017.

Gwyther, D. E., Galton-Fenzi, B. K., Hunter, J. R., and Roberts, J. L.: Simulated melt rates for the Totten and Dalton ice shelves, Ocean Science, 10, 267–279, https://doi.org/10.5194/os-10-267-2014, 2014.

Haran, T., Bohlander, J., Scambos, T., Painter, T., Fahnestock, M.: MODIS Mosaic of Antarctica 2003 – 2004 (MOA2004) Image Map, Version 1. NASA National Snow and Ice Data Center Distributed Active Archive Center [data set], https://doi.org/10.5067/68TBT0CGJSOJ, 2005.

Haran, T., Bohlander, J., Scambos, T., Painter, T., Fahnestock, M.: MODIS Mosaic of Antarctica 2008 – 2009 (MOA2009) Image Map, Version 1. NASA National Snow and Ice Data Center Distributed Active Archive Center [data set], https://doi.org/10.5067/4ZL43A4619AF, 2014.

Haran, T., Linger, M., Bohlander, J., Fahnestock, M., Painter, T., Scambos, T.: MEaSUREs MODIS Mosaic of Antarctica 2013-2014 (MOA2014) Image Map, Version 1. NASA National Snow and Ice Data Center Distributed Active Archive Center [data set], https://doi.org/10.5067/RNF17BP824UM, 2018.

Formatted: Font color: Auto
Field Code Changed
Formatted: Font color: Auto
Formatted: Font color: Auto
Field Code Changed
Formatted: Font color: Auto
Formatted: Font color: Auto
Formatted: Font color: Auto
Field Code Changed
Formatted: Font color: Auto
Formatted: Font color: Auto

Harig, C. and Simons, F. J.: Accelerated West Antarctic ice mass loss continues to outpace East Antarctic gains, Earth and Planetary Science Letters, 415, 134–141, https://doi.org/10.1016/j.epsl.2015.01.029, 2015.

Herraiz-Borreguero, L. and Garabato, A. C, N.: Poleward shift of Circumpolar Deep Water threatens the East Antarctic Ice Sheet, Nature Climate Change, 12, 728–734, https://doi.org/10.1038/s41558-022-01424-3, 2022.

Howat, I. M., Porter, C., Smith, B. E., Noh, M.-J., and Morin, P.: The Reference Elevation Model of Antarctica, The Cryosphere, 13, 665–674, https://doi.org/10.5194/tc-13-665-2019, 2019.

Jenkins, A., Dutrieux, P., Jacobs, S. S., McPhail, S. D., Perrett, J. R., Webb, A. T., and White, D.: Observations beneath Pine Island Glacier in West Antarctica and implications for its retreat, Nature Geoscience, 3, 468–472, https://doi.org/10.1038/ngeo890, 2010.

Jordan, J., Miles, B., Gudmundsson, G., Jamieson, S., Jenkins, A., Stokes, C.: Increased warm water intrusions could cause mass loss in East Antarctica during the next 200 years, Nature Communications, 14, 1825, https://doi.org/10.1038/s41467-023-37553-2, 2023.

Joughin, I. and Alley, R. B.: Stability of the West Antarctic ice sheet in a warming world, Nature Geoscience, 4, 506–513, https://doi.org/10.1038/ngeo1194, 2011.

Joughin, I., Smith, B. E., and Medley, B.: Marine Ice Sheet Collapse Potentially Under Way for the Thwaites Glacier Basin, West Antarctica, Science, 344, 735–738, https://doi.org/10.1126/science.1249055, 2014.

Khazendar, A., Schodlok, M. P., Fenty, I., Ligtenberg, S.R.M., Rignot, E., van den Broeke, M.R.: Observed thinning of Totten Glacier is linked to coastal polynya variability, Nature Communications, 4, 2857, 1-9, 2013.

Kim, K., Jezek, K. C., and Liu, H.: Orthorectified image mosaic of Antarctica from 1963 Argon satellite photography: image processing and glaciological applications, International Journal of Remote Sensing, 28, 5357–5373, https://doi.org/10.1080/01431160601105850, 2007.

Konrad, H., Gilbert, L., Cornford, S. L., Payne, A., Hogg, A., Muir, A., and Shepherd, A.: Uneven onset and pace of ice-dynamical imbalance in the Amundsen Sea Embayment, West Antarctica, Geophysical Research Letters, 44, 910–918, https://doi.org/10.1002/2016GL070733, 2017.

Konrad, H., Shepherd, A., Gilbert, L., Hogg, A., McMillan, M., Muir, A., Slater, T.: Net retreat of Antarctic glacier grounding lines, Nature Geoscience, 11, 258-262, https://doi.org/10.1038/s41561-018-0082-z, 2018.

Kusahara, K., Hasumi, H., and Williams, G. D.: Impact of the Mertz Glacier Tongue calving on dense water formation and export, Nature Communications, 2, 159, https://doi.org/10.1038/ncomms1156, 2011.

Lhermitte, S., Sun, S., Shuman, C., Wouters, B., Pattyn, F., Wuite, J., Berthier, E., and Nagler, T.: Damage accelerates ice shelf instability and mass loss in Amundsen Sea Embayment, Proceedings of the National Academy of Sciences, 117, 24735–24741, https://doi.org/10.1073/pnas.1912890117, 2020.

Lee, J., Marotzke, J., Bala, G., Cao, L., Corti, S., Dunne, J., Engelbrecht, F., Fischer, E., Fyfe, J., Jones, C., Maycock, A., Mutemi, J., Ndiaye, O., Panickal, S., Zhou, T.: Chapter 4 - Future Global Climate: Scenario-based Projections and Near-term Information, in: Climate Change 2021: The Physical Science Basis. Contribution of Working Group I to the Sixth Assessment Report of the Intergovernmental Panel on Climate Change, edited by: Masson-Delmotte, V., Zhai, P., Pirani, A., Connors, S., Péan, C., Berger, S., Caud, N., Chen, Y., Goldfarb, L., Gomis, M., Huang, M., Leitzell, K., Lonnoy, E., Matthews, J., Maycock, T., Waterfield, T., Yelekci, O., Yu, R., Zhou, B, Cambridge University Press, Cambridge, 553-672, https://doi.org/10.1017/9781009157896.006, 2021.

Li, X., Rignot, E., Mouginot, J., Scheuchl, B.: Ice flow dynamics and mass loss of Totten Glacier, East Antarctica, from 1989 to 2015, Geophysical Research Letters, 43, 12, 6366-6373, 2016.

Li, R., Lv, D., Xie, H., Tian, Y., Xu, Y., Lu, S., Tong, X., and Weng, H.: A comprehensive assessment and analysis of Antarctic satellite grounding line products from 1992 to 2009, Science China Earth Sciences, 64, 1332–1345, https://doi.org/10.1007/s11430-020-9729-6, 2021.

Li, X., Rignot, E., Morlighem, M., Mouginot, J., and Scheuchl, B.: Grounding line retreat of Totten Glacier, East Antarctica, 1996 to 2013, Geophysical Research Letters, 42, 8049–8056, https://doi.org/10.1002/2015GL065701, 2015.

Lim, E.-P., Hendon, H. H., Arblaster, J. M., Delage, F., Nguyen, H., Min, S.-K., and Wheeler, M. C.: The impact of the Southern Annular Mode on future changes in Southern Hemisphere rainfall, Geophysical Research Letters, 43, 7160–7167, https://doi.org/10.1002/2016GL069453, 2016.

Martín-Español, A., Zammit-Mangion, A., Clarke, P. J., Flament, T., Helm, V., King, M. A., Luthcke, S. B., Petrie, E., Rémy, F., Schön, N., Wouters, B., and Bamber, J. L.: Spatial and temporal Antarctic Ice Sheet mass trends, glacio-isostatic adjustment, and surface processes from a joint inversion of satellite altimeter, gravity, and GPS data, Journal of Geophysical Research: Earth Surface, 121, 182–200, https://doi.org/10.1002/2015JF003550, 2016.

Massom, R., Scambos, T., Bennetts, L., Reid, P., Squire, V., Stammerjohn, S.: Antarctic ice shelf disintegration triggered by sea ice loss and ocean swell, Nature, 558, 383-389, https://doi.org/10.1038/s41586-018-0212-1, 2018.

Field Code Changed

Formatted: Font color: Auto

Formatted: Font color: Auto

Formatted: Font color: Auto

Matsuoka, K., Skoglund, A., Roth, G., de Pomereu, J., Griffiths, H., Headland, R., Herried, B., Katsumata, K., Le Brocq, A., Licht, K., Morgan, F., Neff, P. D., Ritz, C., Scheinert, M., Tamura, T., Van de Putte, A., van den Broeke, M., von Deschwanden, A., Deschamps-Berger, C., Van Liefferinge, B., Tronstad, S., and Melvær, Y.: Quantarctica, an integrated mapping environment for Antarctica, the Southern Ocean, and sub-Antarctic islands, Environmental Modelling & Software, 140, 105015, https://doi.org/10.1016/j.envsoft.2021.105015, 2021.

Mayer, H. and Herzfeld, U. C.: Structural glaciology of the fast-moving Jakobshavn Isbræ, Greenland, compared to the surging Bering Glacier, Alaska, U.S.A., Annals of Glaciology, 30, 243–249, https://doi.org/10.3189/172756400781820543, 2000.

McMillan, M., Shepherd, A., Sundal, A., Briggs, K., Muir, A., Ridout, A., Hogg, A., and Wingham, D.: Increased ice losses from Antarctica detected by CryoSat-2, Geophysical Research Letters, 41, 3899–3905, https://doi.org/10.1002/2014GL060111, 2015.

Medley, B., Joughin, I., Smith, B. E., Das, S. B., Steig, E. J., Conway, H., Gogineni, S., Lewis, C., Criscitiello, A. S., McConnell, J. R., van den Broeke, M. R., Lenaerts, J. T. M., Bromwich, D. H., Nicolas, J. P., and Leuschen, C.: Constraining the recent mass balance of Pine Island and Thwaites glaciers, West Antarctica, with airborne observations of snow accumulation, The Cryosphere, 8, 1375–1392, https://doi.org/10.5194/tc-8-1375-2014, 2014.

Met-READER.: Casey Temperature. British Antarctic Survey [data set] https://legacy.bas.ac.uk/met/READER/surface/Casey.All.temperature.html, 2022.

Miles, B. W. J.: Synchronous terminus change of East Antarctic outlet glaciers linked to climatic forcing. Masters Thesis, Durham University, http://etheses.dur.ac.uk/7333/, 2013.

Miles, B. W. J., Stokes, C. R., Vieli, A., Cox, N.: Rapid, climate-driven changes in outlet glaciers on the Pacific coast of East Antarctica, Nature, 500, 563-566, http://dx.doi.org/10.1038/nature12382, 2013.

Miles, B. W. J., Stokes, C. R., Jamieson, S. S. R.: Pan–ice-sheet glacier terminus change in East Antarctica reveals sensitivity of Wilkes Land to sea-ice changes, Science Advances, 2, 5, 1-7, https://doi.org/10.1126/sciadv.1501350, 2016.

Miles, B. W. J., Stokes, C. R., and Jamieson, S. S. R.: Simultaneous disintegration of outlet glaciers in Porpoise Bay (Wilkes Land), East Antarctica, driven by sea ice break-up, The Cryosphere, 11, 427–442, https://doi.org/10.5194/tc-11-427-2017, 2017.

Miles, B. W. J., Stokes, C. R., and Jamieson, S. S. R.: Velocity increases at Cook Glacier, East Antarctica, linked to ice shelf loss and a subglacial flood event, The Cryosphere, 12, 3123–3136, https://doi.org/10.5194/tc-12-3123-2018, 2018.

Field Code Changed

Formatted: Font color: Auto

Formatted: Font color: Auto

Formatted: Font color: Auto

Miles, B. W. J., Jordan, J. R., Stokes, C. R., Jamieson, S. S. R., Gudmundsson, G. H., and Jenkins, A.: Recent acceleration of Denman Glacier (1972–2017), East Antarctica, driven by grounding line retreat and changes in ice tongue configuration, The Cryosphere, 15, 663–676, https://doi.org/10.5194/tc-15-663-2021, 2021.

Miles, B. W. J., Stokes, C. R., Jenkins, A., Jordan, J. R., Jamieson, S. S. R., and Gudmundsson, G. H.: Slowdown of Shirase Glacier caused by strengthening alongshore winds, The Cryosphere Discussions, 1–19, https://doi.org/10.5194/tc-2022-126, 2022.

Milillo, P., Rignot, E., Rizzoli, P., Scheuchl, B., Mouginot, J., Bueso-Bello, J., and Prats-Iraola, P.: Heterogeneous retreat and ice melt of Thwaites Glacier, West Antarctica, Science Advances, 5, eaau3433, https://doi.org/10.1126/sciadv.aau3433, 2019.

Millan, R., Mouginot, J., Derkacheva, A., Rignot, E., Milillo, P., Ciraci, E., Dini, L., and Bjørk, A.: Ongoing grounding line retreat and fracturing initiated at the Petermann Glacier ice shelf, Greenland, after 2016, The Cryosphere, 16, 3021–3031, https://doi.org/10.5194/tc-16-3021-2022, 2022.

Mohajerani, Y., Jeong, S., Scheuchl, B., Velicogna, I., Rignot, E., and Milillo, P.: Automatic delineation of glacier grounding lines in differential interferometric synthetic-aperture radar data using deep learning, Scientific Reports, 11, 4992, https://doi.org/10.1038/s41598-021-84309-3, 2021.

Moon, T. and Joughin, I.: Changes in ice front position on Greenland's outlet glaciers from 1992 to 2007, Journal of Geophysical Research: Earth Surface, 113, 1-10, https://doi.org/10.1029/2007JF000927, 2008.

Moon, T., Joughin, I., and Smith, B.: Seasonal to multiyear variability of glacier surface velocity, terminus position, and sea ice/ice mélange in northwest Greenland, Journal of Geophysical Research: Earth Surface, 120, 818–833, https://doi.org/10.1002/2015JF003494, 2015.

Morlighem, M.: MEaSUREs BedMachine Antarctica, Version 2. NASA National Snow and Ice Data Center Distributed Active Archive Center [data set], https://doi.org/10.5067/E1QL9HFQ7A8M, 2020.

Morlighem, M., Rignot, E., Binder, T., Blankenship, D., Drews, R., Eagles, G., Eisen, O., Ferraccioli, F., Forsberg, R., Fretwell, P., Goel, V., Greenbaum, J. S., Gudmundsson, H., Guo, J., Helm, V., Hofstede, C., Howat, I., Humbert, A., Jokat, W., Karlsson, N. B., Lee, W. S., Matsuoka, K., Millan, R., Mouginot, J., Paden, J., Pattyn, F., Roberts, J., Rosier, S., Ruppel, A., Seroussi, H., Smith, E. C., Steinhage, D., Sun, B., Broeke, M. R. van den, Ommen, T. D. van, Wessem, M. van, and Young, D. A.: Deep glacial troughs and stabilizing ridges unveiled beneath the margins of the Antarctic ice sheet, Nature Geoscience, 13, 132–137, https://doi.org/10.1038/s41561-019-0510-8, 2020.

Field Code Changed
Formatted: Font color: Auto
Formatted: Font color: Auto
Formatted: Font color: Auto

Mouginot, J., Rignot, E., and Scheuchl, B.: Sustained increase in ice discharge from the Amundsen Sea Embayment, West Antarctica, from 1973 to 2013, Geophysical Research Letters, 41, 1576–1584, https://doi.org/10.1002/2013GL059069, 2014.

Nagler, T., Rott, H., Hetzenecker, M., Wuite, J., and Potin, P.: The Sentinel-1 Mission: New Opportunities for Ice Sheet Observations, Remote Sensing, 7, 9371–9389, https://doi.org/10.3390/rs70709371, 2015.

Nagler, T., Wuite, J., Libert, L., Hetzenecker, M., Keuris, L., Rott, H.: Continuous Monitoring of Ice Motion and Discharge of Antarctic and Greenland Ice Sheets and Outlet Glaciers by Sentinel-1 A & B, IEEE International Geoscience and Remote Sensing Symposium IGARSS, 1061-1064, https://doi.org/10.1109/IGARSS47720.2021.9553514, 2021.

Nias, I. J., Cornford, S. L., and Payne, A. J.: Contrasting the modelled sensitivity of the Amundsen Sea Embayment ice streams, Journal of Glaciology, 62, 552–562, https://doi.org/10.1017/jog.2016.40, 2016.

Nicholls, K., Corr, H., Stewart, C., Lok, L., Brennan, P., Vaughan, D.: Instruments and Methods: A ground-based radar for measuring vertical strain rates and time-varying basal melt rates in ice sheets and shelves, Journal of Glaciology, 61, 230, 1079-1087, https://doi.org/10.3189/2015JoG15J073, 2015.

Nilsson, J., Gardner, A. S., and Paolo, F. S.: Elevation change of the Antarctic Ice Sheet: 1985 to 2020, Earth System Science Data, 14, 3573–3598, https://doi.org/10.5194/essd-14-3573-2022, 2022.

Paolo, F. S., Fricker, H. A., Padman, L. Volume loss from Antarctic ice shelves is accelerating, Science, 348, 6232, 327-331, https://doi.org/10.1126/science.aaa0940, 2015.

Parizek, B. R., Christianson, K., Anandakrishnan, S., Alley, R. B., Walker, R. T., Edwards, R. A., Wolfe, D. S., Bertini, G. T., Rinehart, S. K., Bindschadler, R. A., and Nowicki, S. M. J.: Dynamic (in)stability of Thwaites Glacier, West Antarctica, Journal of Geophysical Research: Earth Surface, 118, 638–655, https://doi.org/10.1002/jgrf.20044, 2013.

Park, J., Gourmelen, N., Shepherd, A., Kim, S., Vaughan, D., Wingham, D.: Sustained retreat of the Pine Island Glacier, Geophysical Research Letters, 40, 2137-2142, https://doi.org/10.1002/grl.50379, 2013.

Pattyn, F. and Derauw, D.: Ice-dynamic conditions of Shirase Glacier, Antarctica, inferred from ERS SAR interferometry, Journal of Glaciology, 48, 559–565, https://doi.org/10.3189/172756502781831115, 2002.

Pattyn, F. and Morlighem, M.: The uncertain future of the Antarctic Ice Sheet, Science, 367, 6484, 1331-1335, https://doi.org/10.1126/science.aaz5487, 2020.

Paul, F., Bolch, T., Briggs, K., Kääb, A., McMillan, M., McNabb, R., Nagler, T., Nuth, C., Rastner, P., Strozzi, T., and Wuite, J.: Error sources and guidelines for quality assessment of glacier area, elevation change, and velocity products derived from satellite data in the Glaciers_cci project, Remote Sensing of Environment, 203, 256–275, https://doi.org/10.1016/j.rse.2017.08.038, 2017.

Pelle, T., Morlighem, M., Nakayama, Y., and Seroussi, H.: Widespread Grounding Line Retreat of Totten Glacier, East Antarctica, Over the 21st Century, Geophysical Research Letters, 48, e2021GL093213, 1-11, https://doi.org/10.1029/2021GL093213, 2021.

Petty, A. A., Holland, P. R., and Feltham, D. L.: Sea ice and the ocean mixed layer over the Antarctic shelf seas, The Cryosphere, 8, 761–783, https://doi.org/10.5194/tc-8-761-2014, 2014.

Pritchard, H. D., Arthern, R. J., Vaughan, D. G., and Edwards, L. A.: Extensive dynamic thinning on the margins of the Greenland and Antarctic ice sheets, Nature, 461, 971–975, https://doi.org/10.1038/nature08471, 2009.

Reese, R., Gudmundsson, G. H., Levermann, A., and Winkelmann, R.: The far reach of ice-shelf thinning in Antarctica, Nature Clim Change, 8, 53–57, https://doi.org/10.1038/s41558-017-0020-x, 2018.

Ribeiro, N., Herraiz-Borreguero, L., Rintoul, S. R., McMahon, C. R., Hindell, M., Harcourt, R., and Williams, G.: Warm Modified Circumpolar Deep Water Intrusions Drive Ice Shelf Melt and Inhibit Dense Shelf Water Formation in Vincennes Bay, East Antarctica, Journal of Geophysical Research: Oceans, 126, 1-17, e2020JC016998, https://doi.org/10.1029/2020JC016998, 2021.

Rignot, E.: Tidal motion, ice velocity and melt rate of Petermann Gletscher, Greenland, measured from radar interferometry, Journal of Glaciology, 42, 476–485, https://doi.org/10.3189/S0022143000003464, 1996.

Rignot, E., Mouginot, J., and Scheuchl, B.: Antarctic grounding line mapping from differential satellite radar interferometry, Geophysical Research Letters, 38, 10, 1-6, https://doi.org/10.1029/2011GL047109, 2011.

Rignot, E., Jacobs, S., Mouginot, J., and Scheuchl, B.: Ice-Shelf Melting Around Antarctica, Science, 341, 266–270, https://doi.org/10.1126/science.1235798, 2013.

Rignot, E., Mouginot, J., Morlighem, M., Seroussi, H., and Scheuchl, B.: Widespread, rapid grounding line retreat of Pine Island, Thwaites, Smith, and Kohler glaciers, West Antarctica, from 1992 to 2011, Geophysical Research Letters, 41, 3502–3509, https://doi.org/10.1002/2014GL060140, 2014.

Deleted: Reeh, N., Thomsen, H. H., Higgins, A. K., and Weidick, A.: Sea ice and the stability of north and northeast Greenland floating glaciers, Annals of Glaciology, 33, 474–480, https://doi.org/10.3189/172756401781818554, 2001.¶

Rignot, E., Mouginot, J., Scheuchl, B.: MEaSUREs Antarctic Grounding Line from Differential Satellite Radar Interferometry, Version 2. NASA National Snow and Ice Data Center Distributed Active Archive Center [data set], https://doi.org/10.5067/IKBWW4RYHF1Q, 2016.

Rignot, E., Mouginot, J., Scheuchl, B., van den Broeke, M., van Wessem, M. J., and Morlighem, M.: Four decades of Antarctic Ice Sheet mass balance from 1979–2017, Proc Natl Acad Sci USA, 116, 1095–1103, https://doi.org/10.1073/pnas.1812883116, 2019.

Roberts, J., Galton-Fenzi, B. K., Paolo, F. S., Donnelly, C., Gwyther, D. E., Padman, L., Young, D., Warner, R., Greenbaum, J., Fricker, H. A., Payne, A. J., Cornford, S., Le Brocq, A., van Ommen, T., Blankenship, D., and Siegert, M. J.: Ocean forced variability of Totten Glacier mass loss, Geological Society, London, Special Publications, 461, 175–186, https://doi.org/10.1144/SP461.6, 2018.

Scambos, T. A., Haran, T. M., Fahnestock, M. A., Painter, T. H., and Bohlander, J.: MODIS-based Mosaic of Antarctica (MOA) data sets: Continent-wide surface morphology and snow grain size, Remote Sensing of Environment, 111, 242–257, https://doi.org/10.1016/j.rse.2006.12.020, 2007.

Scambos, T. A., Bell, R. E., Alley, R. B., Anandakrishnan, S., Bromwich, D. H., Brunt, K., Christianson, K., Creyts, T., Das, S. B., DeConto, R., Dutrieux, P., Fricker, H. A., Holland, D., MacGregor, J., Medley, B., Nicolas, J. P., Pollard, D., Siegfried, M. R., Smith, A. M., Steig, E. J., Trusel, L. D., Vaughan, D. G., and Yager, P. L.: How much, how fast?: A science review and outlook for research on the instability of Antarctica's Thwaites Glacier in the 21st century, Global and Planetary Change, 153, 16–34, https://doi.org/10.1016/j.gloplacha.2017.04.008, 2017.

Schoof, C.: Ice sheet grounding line dynamics: Steady states, stability, and hysteresis, Journal of Geophysical Research: Earth Surface, 112, 1-19, https://doi.org/10.1029/2006JF000664, 2007.

Schröder, L., Horwath, M., Dietrich, R., Helm, V., van den Broeke, M. R., and Ligtenberg, S. R. M.: Four decades of Antarctic surface elevation changes from multi-mission satellite altimetry, The Cryosphere, 13, 427–449, https://doi.org/10.5194/tc-13-427-2019, 2019.

Shean, D., Joughin, I., Dutrieux, P., Smith, B., Berthier, E.: Ice shelf basal melt rates from a high-resolution digital elevation model (DEM) record for Pine Island Glacier, Antarctica, The Cryosphere, 13, 2633–2656, https://doi.org/10.5194/tc-13-2633-2019, 2019.

Field Code Changed

Formatted: Font color: Auto

Formatted: Font color: Auto

Shen, Q., Wang, H., Shum, C. K., Jiang, L., Hsu, H. T., and Dong, J.: Recent high-resolution Antarctic ice velocity maps reveal increased mass loss in Wilkes Land, East Antarctica, Scientific Reports, 8, 4477, 1-8, https://doi.org/10.1038/s41598-018-22765-0, 2018.

Shepherd, A., Gilbert, L., Muir, A. S., Konrad, H., McMillan, M., Slater, T., Briggs, K. H., Sundal, A. V., Hogg, A. E., and Engdahl, M. E.: Trends in Antarctic Ice Sheet Elevation and Mass, Geophysical Research Letters, 46, 8174–8183, https://doi.org/10.1029/2019GL082182, 2019.

Smith, B., Fricker, H. A., Gardner, A. S., Medley, B., Nilsson, J., Paolo, F. S., Holschuh, N., Adusumilli, S., Brunt, K., Csatho, B., Harbeck, K., Markus, T., Neumann, T., Siegfried, M. R., and Zwally, H. J.: Pervasive ice sheet mass loss reflects competing ocean and atmosphere processes, Science, 368, 1239–1242, https://doi.org/10.1126/science.aaz5845, 2020.

Spence, P., Griffies, S. M., England, M. H., Hogg, A. McC., Saenko, O. A., and Jourdain, N. C.: Rapid subsurface warming and circulation changes of Antarctic coastal waters by poleward shifting winds, Geophysical Research Letters, 41, 4601–4610, https://doi.org/10.1002/2014GL060613, 2014.

Steig, E. J., Ding, Q., Battisti, D. S., and Jenkins, A.: Tropical forcing of Circumpolar Deep Water Inflow and outlet glacier thinning in the Amundsen Sea Embayment, West Antarctica, Annals of Glaciology, 53, 19–28, https://doi.org/10.3189/2012AoG60A110, 2012.

Stokes, C. R., Abram, N. J., Bentley, M. J., Edwards, T. L., England, M. H., Foppert, A., Jamieson, S. S. R., Jones, R. S., King, M. A., Lenaerts, J. T. M., Medley, B., Miles, B. W. J., Paxman, G. J. G., Ritz, C., van de Flierdt, T., and Whitehouse, P. L.: Response of the East Antarctic Ice Sheet to past and future climate change, Nature, 608, 275–286, https://doi.org/10.1038/s41586-022-04946-0, 2022.

Sun, S., Cornford, S. L., Gwyther, D. E., Gladstone, R. M., Galton-Fenzi, B. K., Zhao, L., and Moore, J. C.: Impact of ocean forcing on the Aurora Basin in the 21st and 22nd centuries, Annals of Glaciology, 57, 79–86, https://doi.org/10.1017/aog.2016.27, 2016.

Sutterley, T. C., Velicogna, I., Rignot, E., Mouginot, J., Flament, T., van den Broeke, M. R., van Wessem, J. M., and Reijmer, C. H.: Mass loss of the Amundsen Sea Embayment of West Antarctica from four independent techniques, Geophysical Research Letters, 41, 8421–8428, https://doi.org/10.1002/2014GL061940, 2014.

The IMBIE Team.: Mass balance of the Antarctic Ice Sheet from 1992 to 2017, Nature, 558, 7709, 219-222, https://doi.org/10.1038/s41586-018-0179-y, 2018.

Thoma, M., Jenkins, A., Holland, D., and Jacobs, S.: Modelling Circumpolar Deep Water intrusions on the Amundsen Sea continental shelf, Antarctica, Geophysical Research Letters, 35, https://doi.org/10.1029/2008GL034939, 2008.

Thompson, A. F., Stewart, A. L., Spence, P., and Heywood, K. J.: The Antarctic Slope Current in a Changing Climate, Reviews of Geophysics, 56, 741–770, https://doi.org/10.1029/2018RG000624, 2018.

Turner, J., Orr, A., Gudmundsson, G. H., Jenkins, A., Bingham, R. G., Hillenbrand, C.-D., and Bracegirdle, T. J.: Atmosphere-ocean-ice interactions in the Amundsen Sea Embayment, West Antarctica, Reviews of Geophysics, 55, 235–276, https://doi.org/10.1002/2016RG000532, 2017a.

Turner, J., Phillips, T., Marshall, G. J., Hosking, J. S., Pope, J. O., Bracegirdle, T. J., and Deb, P.: Unprecedented springtime retreat of Antarctic sea ice in 2016, Geophysical Research Letters, 44, 6868–6875, https://doi.org/10.1002/2017GL073656, 2017b.

Turner, J., Holmes, C., Caton Harrison, T., Phillips, T., Jena, B., Reeves-Francois, T., Fogt, R., Thomas, E. R., and Bajish, C. C.: Record Low Antarctic Sea Ice Cover in February 2022, Geophysical Research Letters, 49, e2022GL098904, 1-11, https://doi.org/10.1029/2022GL098904, 2022.

Vaňková, I., Cook, S., Winberry, P., Nicholls, K., Galton-Fenzi, B.: Deriving Melt Rates at a Complex Ice Shelf Base Using In Situ Radar: Application to Totten Ice Shelf, Geophysical Research Letters, 48, e2021GL092692, 1-10, https://doi.org/10.1029/2021GL092692, 2021.

Wang, L., Davis, J. L., and Howat, I. M.: Complex Patterns of Antarctic Ice Sheet Mass Change Resolved by Time-Dependent Rate Modeling of GRACE and GRACE Follow-On Observations, Geophysical Research Letters, 48, e2020GL090961, https://doi.org/10.1029/2020GL090961, 2021.

Winsborrow, M. C. M., Clark, C. D., and Stokes, C. R.: What controls the location of ice streams?, Earth-Science Reviews, 103, 45–59, https://doi.org/10.1016/j.earscirev.2010.07.003, 2010.

Yamazaki, K., Aoki, S., Katsumata, K., Hirano, D., and Nakayama, Y.: Multidecadal poleward shift of the southern boundary of the Antarctic Circumpolar Current off East Antarctica, Science Advances, 7, eabf8755, https://doi.org/10.1126/sciadv.abf8755, 2021.

Young, D. A., Wright, A. P., Roberts, J. L., Warner, R. C., Young, N. W., Greenbaum, J. S., Schroeder, D. M., Holt, J. W., Sugden, D. E., Blankenship, D. D., van Ommen, T. D., and Siegert, M. J.: A dynamic early East Antarctic Ice Sheet suggested by ice-covered fjord landscapes, Nature, 474, 72–75, https://doi.org/10.1038/nature10114, 2011.

Formatted: Font color: Auto

Yu, H., Rignot, E., Seroussi, H., and Morlighem, M.: Retreat of Thwaites Glacier, West Antarctica, over the next 100 years using various ice flow models, ice shelf melt scenarios and basal friction laws, The Cryosphere, 12, 3861–3876, https://doi.org/10.5194/tc-12-3861-2018, 2018.

Zheng, F., Li, J., Clark, R. T., and Nnamchi, H. C.: Simulation and Projection of the Southern Hemisphere Annular Mode in CMIP5 Models, Journal of Climate, 26, 9860–9879, https://doi.org/10.1175/JCLI-D-13-00204.1, 2013.